Summary

Introduction 3

Section 1

1. Introduction to Photovoltaics..... 5
2. The light..... 11
3. Light trapping absorption and optical losses 15
4. Structure and properties of silicon..... 23
   4.1. Design rules of crystalline silicon 24
   4.2. High efficiency concepts of c-Si wafer..... 29
5. Heterojunction solar cells 33

Section 2

1. Comparative study on renewable energy subsiding systems between Italy and Turkey 49
   1.1. Feed-in scheme(Conto Energia) 49
   1.2. First Feed-in scheme 49
   1.3. Second Feed-in scheme 50
   1.4. Third Feed-in scheme..... 52
   1.4.1. Awards..... 54
   1.4.2 Integrated PV Plants with Innovative Features 55
   1.4.3. Concentrated Photovoltaic Plants (CPV) 55
   1.5. Fourth feed-in tariff scheme 56
   1.5.1. Ranking system and restrictions for large PV plants 58
   1.6. Fifth feed in scheme..... 59
   1.6.1 Access to incentives 60
   1.6.2. Access through the GSE ranking system 60
   1.7. Results of the Italian system 62
   1.8. Turkey subsidies system 64
   1.9. Results of Turkish subsiding system 66

Section 3

1. Wireless charger 69
1.1. Coupling 72
2. The project of the charger 75
3. Results 77
3.1. Inverter 77
3.2.Rectangular coil 79
First test 79
Second test 81
Third test 82
Fourth and fifth test 83
13. Compensation 87
Conclusions 89
Riassunto 91
Bibliography 93

Introduction

My thesis is focused on PV technologies theory and their application. The present research embeds such a multi-perspective approach through a tripartite structure that will respectively cover: the history and development of PV technologies in the first section, a comparative study about PV technologies implementation between Italy and Turkey (where I conducted field research) in the second section, and the designing and projecting and of a wireless charger in the third section.

For almost two decades photovoltaic has been one of the most popular field of research. In the initial section of work I will introduce the most used and studied innovations among photovoltaic technologies. I will start in chapter one by introducing the photovoltaic effect by using crucial points and explaining the categorization of different technologies according to PV generations. As the work will develop, the main ıssues, of the photovoltaic technology will be introduced and offering also perspectives on remedies to these defects.

In this first section the development and implementation of the photovoltaic technology in history will be easily tracked down thanks to the support of charts and graphs.

The concept related to light, light trapping absorption and optical losses will be extensively explained and described in the second paragraph of the first section. It will be possible to realize what light is and how it propagates through space and other different bodies. It will also draw an explanatory framework necessary to understand which part of the light spectrum produces the photovoltaic effect and which part of the light spectrum can be effectively utilized. Furthermore, it will be taken into account how the material respond when the light affect them.

Moreover, section one will follow with a fourth paragraph in which photon absorption material such as Silicon will be deeply explained; its structure and properties and designing will be analyzed . Furthermore, all improving techniques will be mentioned and described highlighting in which manner they contribute to increase the efficiency of the conversion.

Paragraphs from five to seven of section one will describe the most recent technologies such as heterojunction solar cells and materials based on Perovskite. The latter, in particular will be illustrated in more detail because of its recent history and fast development.

The eight and last paragraph of the first section will explain the status and prospect of solar energy with several comparisons between countries and their energy mix.

Section two of my study is related to the context in which I studied and conducted my research for the past six months. It will treat the comparison between Italian and Turkish subsiding system in order to help building awareness on how this technology could and should be promoted for a wider spread.

Ultimately, section three of my study will be dedicated to my project. In this section I describe the design of the prototype of wireless charger for electrical car battery charging supplying charts and pictures. I will search for the optimal size and shape of primary and secondary coils with the aim to maximize power transmission. Results will be transcribed and conclusions drawn.

Section 1

1. Introduction to Photovoltaics

The process in which solar light is directly converted into voltage or current is named the photovoltaic (PV) effect. It is shown below in a simplified representation of a silicon based solar cell (Figure 1.0). It consists of the c-Si absorber layer, a pn-junction to separate the light excited charge carriers and a metal front grid contact and back contact.

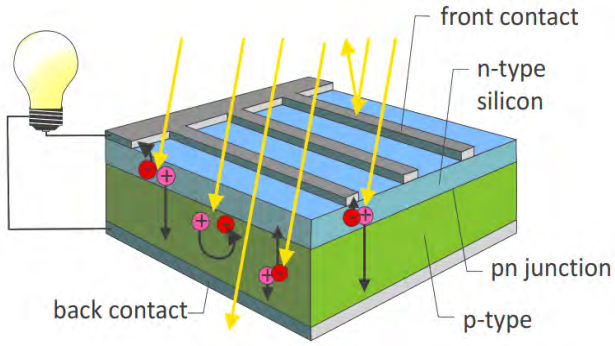

Figure 1.0 Simplified silicon based solar cell

The light affects the solar cell from the front side, that in Figure 1.0 is the side on the top. Then the light's energy is absorbed into the absorber layer. This energy is used to excite charge carriers in the semiconductor material, which are respectively: a negatively charged electron, indicated by the red dot, and a positively charged hole, indicated by the blue dot. In other words when the photon is absorbed it leads to the creation of a pair of electron-hole. The radiative energy is converted into chemical energy of the electron-hole pair. These charge carriers diffuse into the cell and need to be separated, which occurs at the depletion region between the n- and p-type doped silicon and the depletion region at the back of the solar cell. At this point, the charge carriers have to be collected at the contacts. The electron will move through the load back to the solar cell.

It is shown that the photovoltaic process is based on three important principles:

- excitation of free mobile charge carriers due to light absorption
- separation of the charge carriers
- collection of the charge carriers at the contacts.

A variety of PV technologies exists today and we can categorize them in various ways. It is possible to categorize them according to the a*bsorber material.* While another categorization approach, often used in books about PV technology is based on the generations. Categorization based on the generations is able to show the progress of the technology.

For this last reason I use the Figure 1.1 in which I plot on the horizontal axis the cost-price of the solar cell per area, expressed in dollar per square meter. In conclusion, if cells are made of expensive materials or using expensive processing methods will be further to the right on this axis. Energy conversion efficiency (η) is the ratio between the useful output of an energy conversion machine and the input, in

energy terms. The conversion efficiency for the solar systems, is the fraction of the energy in the solar light, which is converted into electricity, which is represented by the vertical axis. Photons can only be absorbed if electron energy levels Ei and Ef are present so that their difference equals to the photon energy, hv = Ef - Ei. Generated power depends on the efficiency: the larger the efficiency is, the larger power per area will be generated. This power is expressed in watts per square meters and the usual standard test conditions for solar cells are:

- 1000W/m^2 for solar irradiation
- 25°C ambient temperature

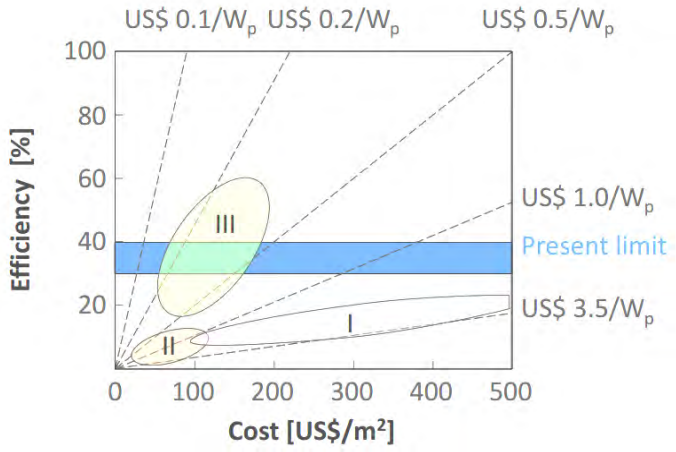

Figure 1.1 Generations of PV

Hence, it is possible to produce 100W per square meter under standard conditions with 10% of conversion efficiency. If the irradiance increases, it is possible to reduce the area obtaining the same power or to increase the output power level of the PV pant. It is necessary to look on a wide geographic scale to see changes in irradiance terms. Going back to the graph, the slope of the dashed line represents the watt per dollar. The cost price per watt-peak corresponds to the cost price of the energy generated by the solar cell. As it is shown in the graph, if the slope of these dashed lines is very steep, the cost price per watt is low, whereas when the slope of the dashed lines becomes less steep the cost price per watt-peak is getting significantly higher. To be compared with other energy sources, PV technology must overlap with the steepest dashed line in the graph . The first generation PV technology is based on using very pure bulky semiconductor materials, like crystalline silicon (c-Si).

Pure materials have few defects and in general solar cells with a relative high efficiency can be manufactured. However, high quality materials require more expensive production processes, which in general makes the cost of solar cell larger as well. In Figure 1.1 roughly circle shows the area in which you would find the first generation PV technology.

A thin-film solar cell, is a second generation solar cell that is made by depositing one or more thin layers, or thin film of photovoltaic material on a substrate, such as glass, plastic or metal. Thin-film solar cells are commercially used in several technologies, including cadmium telluride(CdTe), copper indium gallium diselenide (CIGS), and amorphous and other thin-film silicon (a-Si, TF-Si), which will be

described later in my work. The application of a thin film implies that less material is used, which makes the solar cell cheaper.

Secondly, these solar cells are manufactured using cheaper processing technologies. As a consequence, the materials have more defects resulting in lower performances. Although the solar cell efficiency is lower, due to the lower cost price per area, the cost price per watt of the second generation PV technology is significant lower.

The blue area of Figure 1.1 represents the so-called Shockley-Queisser limit. Given the shape of our solar spectrum and the band gap of the materials used, the Shockley-Queisser limit tells us the theoretically maximum conversion efficiency of the solar cell.

Third generation PV technologies are based on solar cell concepts, which try to go beyond the Shockley-Queisser limit. Therefore third generation PV technology are solar cells with higher conversion efficiencies compared to the first and second generations. Furthermore, the cost price of the materials and processing techniques used to process the third generation solar cells are expected to be cheap as well. The result is that the third generation solar cell technology overlaps with the steepest dashed lines in this graph, meaning that third generation technology would have the lowest cost price per wattpeak (Wp).

Even if beating the Shockley-Queisser limit for most concepts is a challenge itself, making these complex concepts cheap is a completely different game. At this current stage, third-generation PV is not at a price point to be able to compete directly with silicon-based cells or the more exotic thin-film technologies, but it will nevertheless play a significant energy role in applications and markets that conventional solar materials will never be able to penetrate. These include low-power consumer electronics and outdoor recreational applications.

Next to categorizing the PV technologies in the three generations, I will indicate the various PV technologies based on the semiconductor material used as absorber layer in the solar cell.

The dominant PV technology is c-Si wafers represented in Figure 1.2. This technology represents around 90% of the current PV market and belongs to the first generation PV technology.

A second based generation PV technology is the thin-film silicon. In this case no c-Si wafers are used but very thin layers of silicon, which are deposited on glass or a flexible substrate. Silicon does not have the same lattice structure and can be amorphous or nanocrystalline.

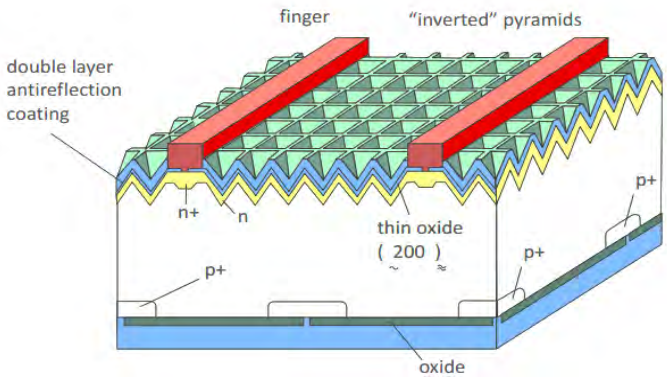

Figure 1.2 c-Si wafers cell

An alternative thin-film PV technology is based on II-VI semiconductor, the cadmium telluride (CdTe) Figure 1.3.

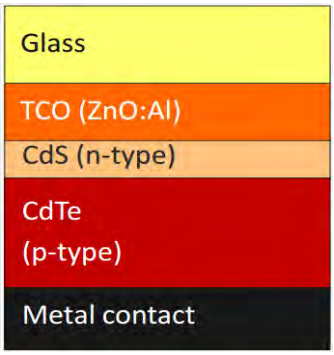

Figure 1.3 Cross-section of Cadmium Telluride cell

CdTe PV technology belongs to the so-called second generation technologies as well. The CdTe has currently the largest market among the thin-film PV technologies. Another thin-film PV technology, based on a chalcogenide alloy is CIGS, which stands for copper indium gallium selenide Figure 1.4. Among the thin-film PV technologies, it has the highest demonstrated conversion efficiency on lab scale, just above 20%. It belongs to the second generation PV technologies as well.

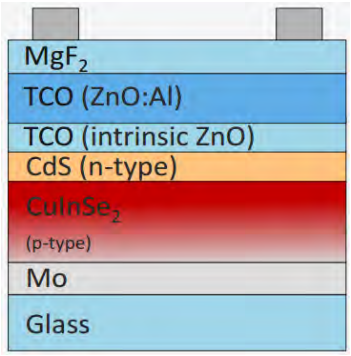

Figure 1.4 Cross-section of CIGS

Moreover, another thin-film PV technology is based on organics, also referred to as the plastic solar cell. The absorption and charge transport in the solar cell occurs in conductive organic polymers or molecules. The dye-sensitized solar cell is a kind of photoelectrochemical system, in which a semiconductor material based on molecular sensitizers is placed between a photo-anode and an electrolyte.

The last PV technology that I will describe is based on III-V semiconductor materials such as gallium arsenide (GaAs). III-V materials are being used in multi-junction devices, often processed on germanium wafers as substrate. The multi-junction devices based on III-V semiconductors are the most efficient solar cells today. The record conversion efficiency of 44% was obtained with a metamorphic triple junction in 2012. The III-V semiconductor solar cells are used in concentrator PV technology and in space applications.

Third generation PV technologies are based on various concepts and try to beat the Shockley-Queisser limit. They also cover a wide range of novel and innovative ideas, the most successful being multi-

junctions. It is also important to realize that most of the previous ideas that I briefly described still need to be proven.

In NREL's chart the progress of all technologies is shown in Figure 1.5. It summarizes the worldwide research effort during the last 40 years and it shows the current record efficiencies of solar cells at research scale. These solar cells are fabricated in a lab environment and are very small in size, often not larger than 1 square centimeter. The purple colored markers represent the III-V technology based on single, double and triple junctions and have efficiencies ranging from 26% up to 44% under concentrated light conditions. The blue lines and dots represent the crystalline silicon technology based on monocrystalline and multicrystalline silicon. The record efficiency ranges from 20% up to 25% under standard 1 sun illumination conditions and 27% can be achieved under 92 sun illumination. The inorganic thin-film technologies, like thin-film silicon, CdTe and CIGS are indicated by the green markers and their record efficiencies range from 13.4 % up to 20%. The red colored lines and marks indicate the emerging PV technologies, like organic solar cells. It must be taken into account that these are lab results of very small area solar cells and this chart does not imply any long term stability data of any PV technologies, especially not of the ones indicated in red. Instead, they indicate the potential efficiency of many PV technologies.

Nevertheless, it is fundamental to remember that most PV technologies still have a large gap between the record conversion efficiency of the lab cells and the conversion efficiency of large commercial modules.

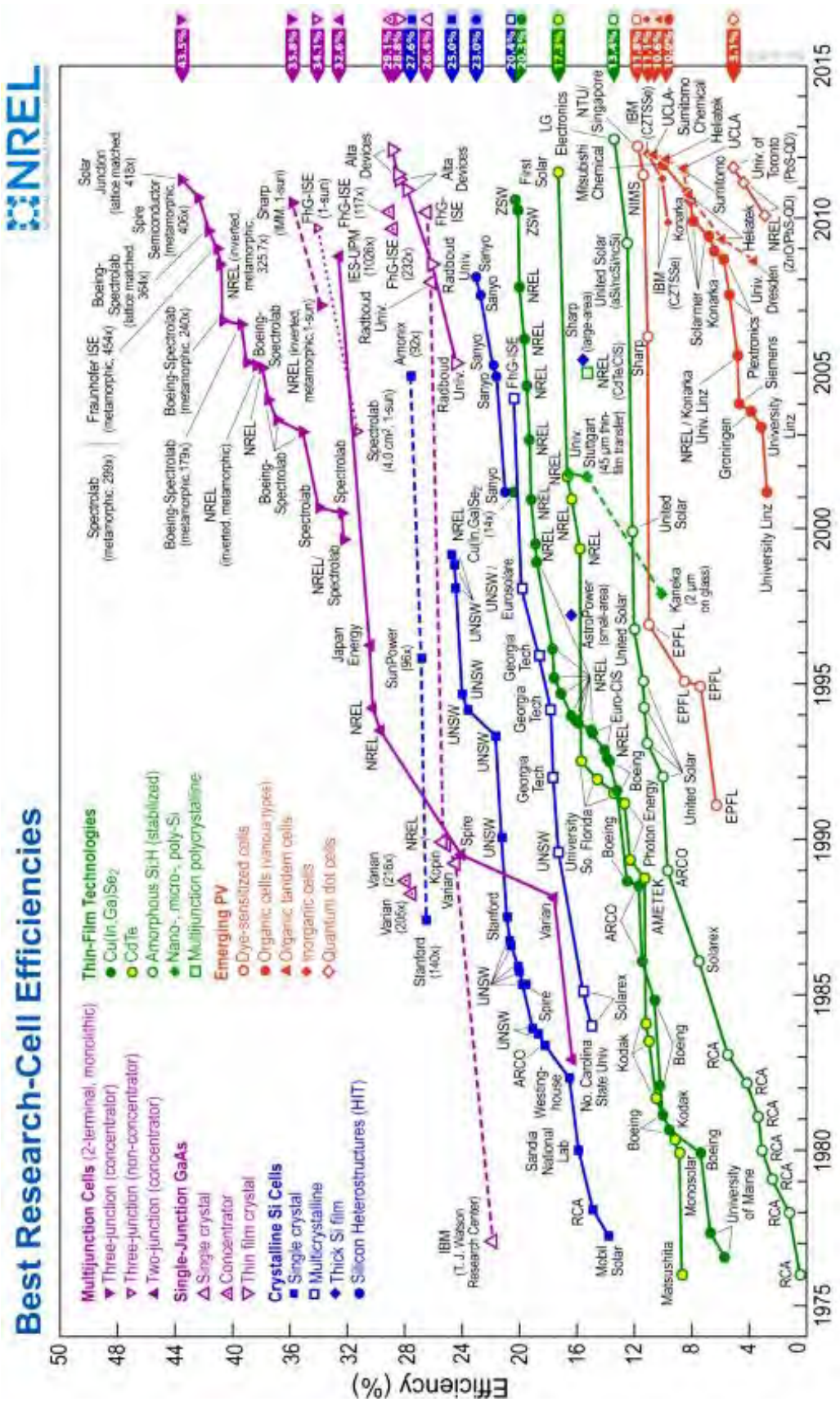

Figure 1.5 NREL's chart

2. The light

In this section I will illustrate and analyze the basic characteristics of light. What is light? What are the physical properties of light? And how does a typical solar spectrum look like?

Light can be described as electromagnetic waves, as well as particles with a quantized amount of energy, which we call a photon (Figure 2.1). First of all, light can be described by a specific kind of particles called photons. It was Einstein who explained photoelectric in his famous paper from 1905[1]. He proposed that light consists of quantized energy packages, which we nowadays call photons. To eject an electron out of the material, it requires a certain threshold energy. The photoelectric effect shows that when the energy of the photons is above this threshold, the charge can be ejected from the material. If the energy is below this threshold no electrons are ejected. This demonstrates that light can be described by photons. Now, we describe light as a wave. Light can be represented by an electromagnetic wave.

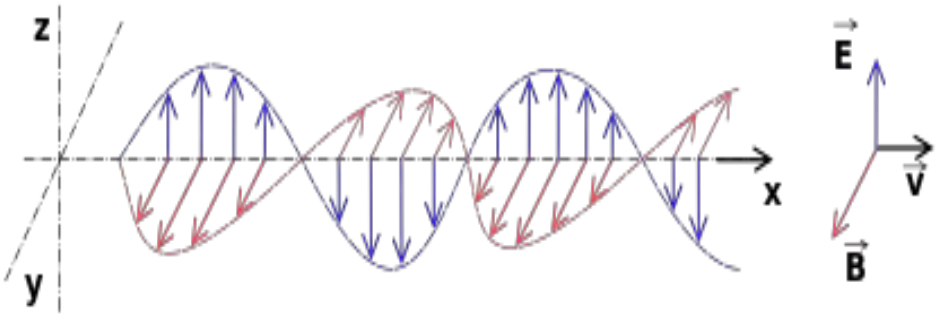

Figure 2.1 Light as a electromagnetic wave

In the image it is represented an electromagnetic wave traveling in direction x. Perpendicular to this direction an electric field E is oscillating. Perpendicular to the direction of propagation and the oscillating electric field, a magnetic field B is oscillating. The distance between the maxima of the oscillating electric field is called the wavelength, usually indicated by the symbol lambda (λ). An electromagnetic wave is propagating with the speed of light c in vacuum.

The frequency and wavelength of waves are related with a simple equation: the velocity of the wave is equal to the product of the frequency (ν) and the wavelength (λ).

$$c = \lambda \nu \qquad (1)$$

[1] "Concerning an Heuristic Point of View Toward the Emission and Transformation of Light", Annalen der Physik 17 (1905): 132-148; "Explanation of the photoelectric effect with use of the quantum hypothesis of Planck" (Light is a flow of corpuscular objects with definite energies - Planck's quanta of energy); "On the Movement of Small Particles Suspended in Stationary Liquids Required by the Molecular-Kinetic Theory of Heat" Annalen der Physik 17 (1905): 549-560; "On the Electrodynamics of Moving Bodies", Annalen der Physik 17 (1905): 891-921, (Invention of the theory of special relativity. Beginnings of the relativistic era in physics); "Does the Inertia of a Body Depend upon its Energy Content?" Annalen der Physik 18 (1905): 639-641 (Invention of the theory of special relativity, E = mc2. Beginnings of the relativistic era in physics).

The energy of the photon with wavelength lambda is equal to the product of the Planck constant h[2] and the frequency.

$$E = h\nu = \frac{hc}{\lambda} \quad (2)$$

As the frequency equals to velocity of light divided by the wavelength, the photon energy can also be expressed in terms of wavelength, it is equal to the product of the Planck constant, the velocity of light divided by the wavelength.

Electromagnetic (EM) waves exist in many spectral ranges. The visible light spectrum in Figure 2.2, which comprises of the electromagnetic waves visible by human eyes, is only a tiny part of the entire spectrum. The visible spectrum ranges from wavelengths of 400 nm up to 700 nm, which corresponds to frequencies in the order of Tera Hz. At the high energetic side of the visible spectrum we find the ultraviolet light, which is constituted by electromagnetic waves with wavelengths in the order of 100 nm. Passing to higher energies we come to consider X-rays which have wavelengths of around 1 nm and Gamma rays which have wavelengths of 0.1 nm.

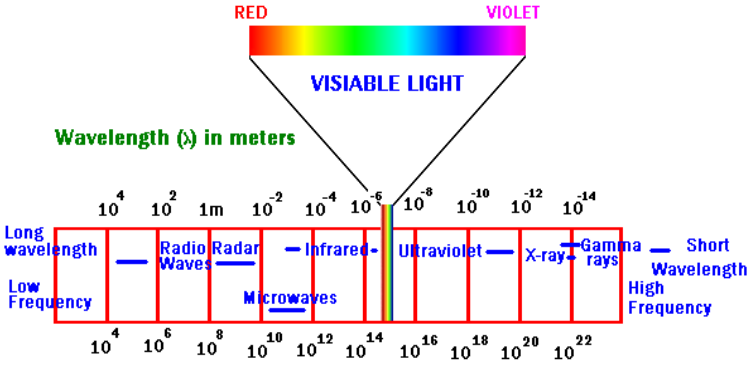

Figure 2.2 The spectrum

On the low energetic side of the visible spectrum we find the infrared light, which has respectively wavelengths of around 1 micron and 10 microns. Microwaves are electromagnetic waves with wavelengths in the order of centimeters. Radio, TV waves are in the order of meters and tens of meters and AM waves in the order of 100 meters. To determine in which spectral range the sun irradiates, I will introduce the quantities irradiance and spectral power density topics.

Firstly, irradiance is the power per unit area and is usually expressed in watts per square meter. As a matter of fact, irradiance does not provide us with any information about the spectral shape of the light source. Secondly, the spectral power density P is a quantity which has spectral information in contrast to the irradiance. The spectral power density is the incident power per unit area and per unit wavelength. The relation between irradiance and spectral power density is constituted by this formula:

$$I = \int_0^{\lambda} P(\lambda) d\lambda \quad (3)$$

[2] The Planck constant denoted h, is a physical constant that is the quantum of action in quantum mechanics. Published in 1900, it originally described the proportionality constant between the energy, E, of a charged atomic oscillator in the wall of a black body, and the frequency, v, of its associated electromagnetic wave.

How does the spectrum of the sun look like, or in other words how does the spectral power density function look like? The sun is a bright object in the sky according to human eyes, yet the sun is a so-called black body radiator.

All matter emits electromagnetic radiation when its temperature is above absolute zero. A body which is not reflective and absorbs all light is called a black body. The spectral power density of a black body radiator which is in thermal equilibrium is given by Planck's law. This law shows that the spectrum peaks at a certain wavelength when the object is at a certain temperature. If a black body radiator has a temperature higher than 500 degrees Celsius, it starts to emit electromagnetic waves in the visible spectrum. The higher the temperature of the black body radiator, the greater the shift of the spectral peak to lower wavelengths (or higher photon energies). Although the sun is not a perfect black body, nor is in thermal equilibrium, Planck's law is a good first estimate of the spectrum of its emitted electromagnetic radiation. The sun's surface is at a temperature of around 5800 Kelvin and therefore its spectral peak is shown in the visible spectrum. If we compare it to planet Earth and consider it as a black body radiator as well, its spectral peak would lie in the infrared region close to 10 microns.

To test solar modules we use so-called solar simulators. We use lamps, which simulate the shape of the solar spectrum. This is far from straightforward since regular lamps have different shaped spectra compared to that of the sun. The lamps are placed in a black box and spectra-shapes are measured using a spectrometer. However, the spectra are quite different from those of the sun. It means that it requires a combination of many types of lamps to simulate the solar spectrum. If we look at the solar spectrum, 9% of its energy is in the ultraviolet (UV) range at wavelengths smaller than 400 nm, 44% of its energy is in the visible range, whereas 47% of its energy is in the infrared Figure 2.3.

Therefore the light can be described as an electromagnetic wave and as a flux of photons. The shape of the spectrum of the sun has been introduced. However, the question is whether this is the solar spectrum arriving at the surface of the Earth and whether it has the same shape and irradiance level.

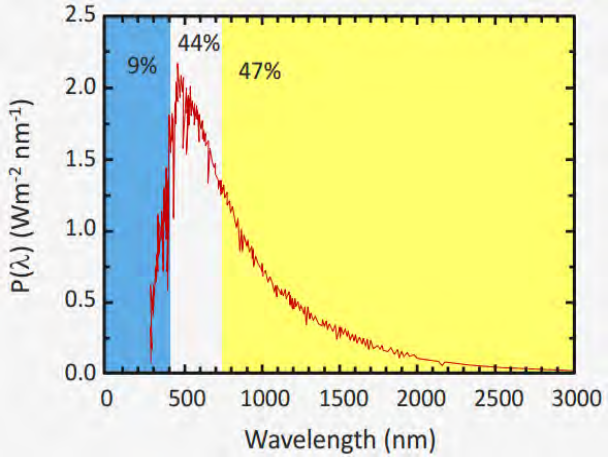

Figure 2.3 Power percentage of solar spectra

3. Light trapping absorption and optical losses

In the ideal solar cell, we want all light that is incident on the solar cell to be absorbed in the absorber layer. How does absorption work? Firstly we have to consider the simple system of a single absorbing medium with a thickness d (Figure 3.1).

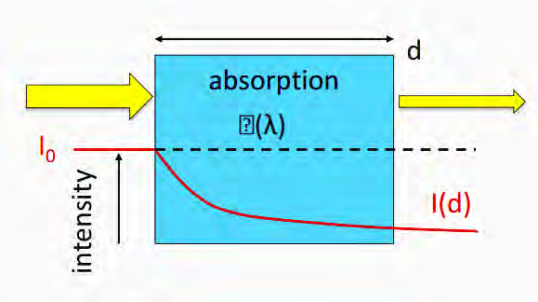

Figure 3.1 Example of absorption characteristic

From the left we have a light ray which is coupled into the film into the x-direction. Part of the light is absorbed in the film. Consider x=0 to be the front side of the medium and x=d is the back side of the medium. At the moment we make a simplification.

First, we neglect the reflection or potential scattering at that interfaces.

Second, we assume the light is monochromatic, which means that all photons have the same energy or wavelength. The absorption of a medium can be defined in terms of an absorption coefficient α. The dimension of the absorption coefficient is one over the length and the typical unit of the absorption coefficient used is one over centimeter. The light intensity drops exponential with distance in the absorber layer. This behavior can be described by the Lambert-Beer's law.

$$\frac{\delta I(v,x)}{\delta x} = -\alpha(v) I(v,x) \quad (4)$$

$$I(v,x) = I_0(v) \exp(-\alpha(v)x) \quad (5)$$

This law states that there is a logarithmic dependence between the intensity of the transmitted light through the layer, the product of the absorption coefficient and the path length. More in depth, over an infinitely small distance dx, the decrease in light intensity due to absorption, *dI/dx*, is equal to the product of the absorption coefficient and the light intensity at position *x*. This is the differential form of the Lambert-Beer's law. Lambert-Beer's law shows that the intensity of light is decreasing exponentially in the x-direction of the absorbing medium. It also means that at the side, at which the light is entering the film, more light is absorbed in reference to the back side.

The total light intensity absorbed in the material is equal to the light intensity entering the absorber layer minus the intensity transmitted through the absorber layer. For a solar cell we would aim to reach 100% absorption. In this condition the absorber would be called *optically thick* that means that the transmission is 0%. From Lambert-Beer's law it can easily be noted that this result can be accomplished by either large values for the thickness d, so very thick films, or large values for the absorption coefficients.

It is important to remember that the absorption coefficient for materials is not the same at every wavelength. In this Figure 3.2 the absorption coefficients for four different semiconductor materials are plotted: Ge (germanium), Si (silicon), GaAs(gallium arsenide) and InP (indium phosphate) .

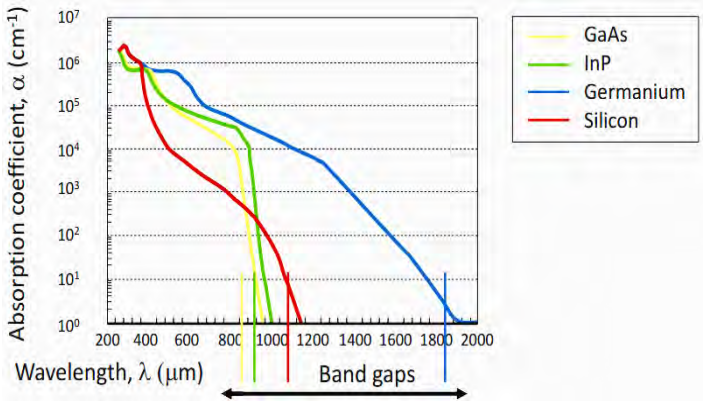

Figure 3.2 Absorption characteristic

Firstly, it can be seen how germanium has the lowest band gap. Germanium starts to absorb at high wavelengths, which is equal to low photon energy. Gallium arsenide has the highest band gap, as it starts to absorb light at the smallest wavelength, or the highest photon energy. Secondly, if we focus on the visible spectral part from 300 nm up to 700 nm, we see that the absorption coefficient of InP and GaAs is significantly higher than the one for silicon. The explanation is that InP and GaAs are direct band gap materials therefore materials with an indirect band gap, like Si and Ge, have smaller absorption coefficients. Only in the very blue part below 400 nm, silicon has a direct band gap transition. Silicon is in fact a relative poor absorber and therefore thicker absorber layers are required in reference to GaAs to absorb the same fraction of light. In general all semiconductor materials show that the absorption coefficient in the blue is orders of magnitude larger than in the red. This means that the penetration depth of blue light into the absorber layer is rather small.

The normalized light intensity with position in the silicon bulk could be useful as an example. As it can be seen in Figure 3.3, the blue light is already fully absorbed within a few nanometers. The red light requires an absorption path length of 60 microns to be fully absorbed. The infrared light is hardly absorbed, and after an optical path length of 100 microns only 10% of the light intensity is absorbed.

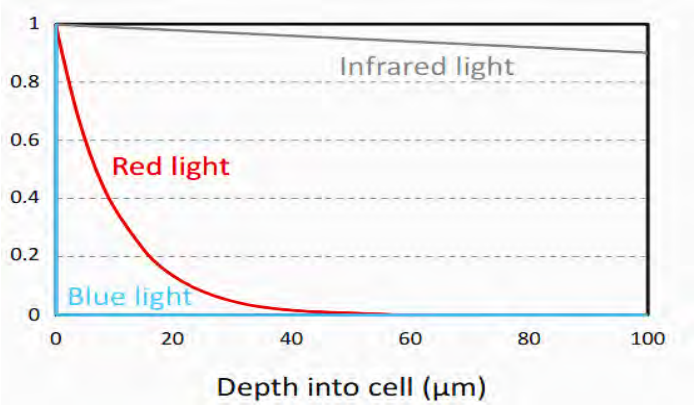

Figure 3.3 Absorption at different wavelength

As the absorption of photons generates excited charge carriers, the wavelength dependence of the absorption coefficient determines the local generation profile of the charge carriers. At the front side where the light enters the absorbing film, the generation of charge carriers is significantly higher than at the back side. It is useful to note some optical loss mechanisms, considering for example a simple crystalline silicon solar cell. The example of the c-Si solar cell shown in this Figure 3.4 , consists of a p-type crystalline silicon bulk with a thin n-type layer on top, named the n-emitter. At the top and the back there are the metal contacts.

In sum, by using this relatively simplified solar cell configuration, we will demonstrate the various optical losses; in other words, which mechanism prevents that all light is being absorbed in the p-type crystalline silicon solar cell.

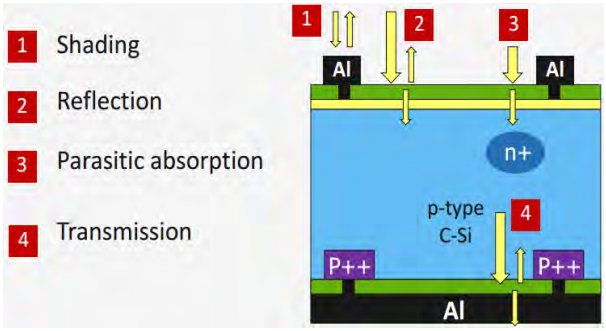

Figure 3.4 Loss mechanism

In order to discuss loss mechanism it might be useful to first consider metal contacts. These type of contacts shade a certain area, preventing light to be absorbed in the PV active layers.

The second optical loss mechanism is the reflection at the front interface of the solar cell. The light passing through an interface between two media with different refractive indices, will always be partly reflected and partly transmitted at the interface.

The third optical loss mechanism is instead constituted by parasitic absorption losses in the non-active PV layers. In this example the green top layer can be an anti-reflection coating or a passivation layer to reduce the number of defects at the surface of the emitter layer. If this layer absorbs photons, these photons will not contribute to charge carrier generation that will be collected at the contacts. This is what we address as parasitic absorption. It means that in a design of solar cells we preferentially would like to use materials for the non-active part of the solar cell that have high transmissions for the spectral part utilized by the solar cell.

Finally, if the absorber layer is not thick enough to absorb all the light, part of the light will be transmitted. This loss mechanism starts to play a role for solar cells based on thin films.

Another topic that is relevant to my work is the way to reduce the reflection at the front surface of a solar cell and how to increase the light trapping in the absorber layers. In the previous section we discussed the optical loss mechanism due to reflection at the front interfaces of a solar cell. The light passing through an interface between two media with different refractive indices, will always be partly reflected and partly transmitted at the interface.

As all types of solar cells suffer from this loss mechanism, antireflection concepts play a major role and are worth being discussed. The fraction of the light intensity that is reflected is given by the Fresnel

coefficients. Consider the interface between two media with refractive index n_1 and n_2. A light ray is arriving with an angle of incidence in reference to the normal of the interface θ_i. Part of the light is reflected under the angle of reflection θ_r. The angle of reflection is equal to the angle of incidence. The light transmitted travels further under the angle of transmission $_t$ to the normal.

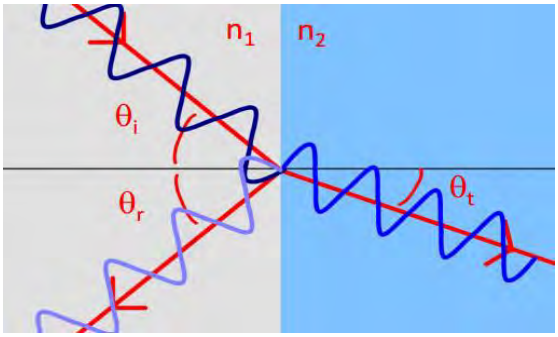

Figure 3.5 Components of a beam of light

The relation between the angle of incidence and transmission is given by Snell's law. If refractive index of medium 1 is smaller than that of medium 2, the angle of transmittance will be smaller than the angle of incidence. If the refractive index of medium 1 is larger than that of medium 2 it is the other way around.

$n_1 \sin_i = n_2 \sin_t$ (6)

$\theta_i = \theta_r$ (7)

The reflection coefficients are given by the Fresnel equations, which are functions of the refractive indices of both media, and the angle of incidence and reflection. The transmission is one minus the reflection. Fresnel equations for transmission and reflection of the p-polarized light are slightly different from those of the s-polarized light. For light with a perpendicular incidence, that is an angle of incidence of zero degrees, the reflection and transmission are equal. In this Figure 3.6 it is shown the relation between the reflection coefficient for s and p-polarized light when the medium 1 has a refractive index of 1 (which is equal to air) and medium 2 has a refractive index of 1.5 (like glass).

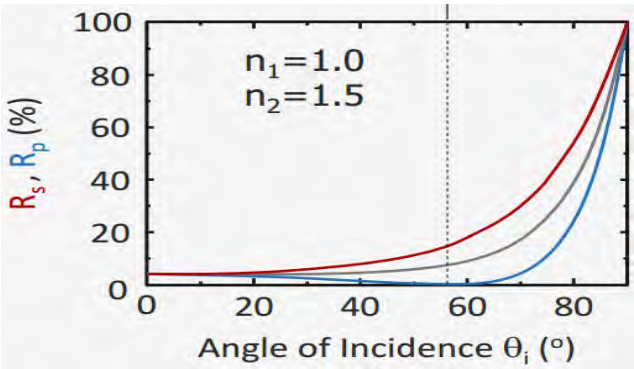

Figure 3.6 R and S polarized light

From the image we can see that the p-polarized light has an angle at which the reflection is equal to zero. This angle is called the Brewster angle. The grey line is the average which represents randomly polarized light. If we look at light rays going from a material with a higher refractive index to a material with a

lower refractive index, we see that the reflection becomes 100% above a certain angle. This is called a total internal reflection and occurs above the critical angle of incidence, which can easily be calculated using Snell's law.

Using these basics, it is possible to look at the interface of silicon, the most common used material for solar cells. Consider an air-silicon interface and for simplicity light under a perpendicular incidence at a wavelength of 500 nm. The refractive index of air is 1 and that of silicon is 4.3 at a wavelength of 500 nm. The Fresnel coefficients (8) and (9) tell us that the optical losses due to reflection are significant at this interface, the reflection is 38.8%.

$$R_p = \left(\frac{n_1\, cos(\theta t) - n_1\, cos(\theta i)}{n_1\, cos(\theta t) + n_1\, cos(\theta i)}\right)^2 \quad (8)$$

$$R_s = \left(\frac{n_1\, cos(\theta i) - n_1\, cos(\theta t)}{n_1\, cos(\theta i) + n_1\, cos(\theta t)}\right)^2 \quad (9)$$

Reduction of this reflection can be achieved by introducing an interlayer with a refractive index n_1 with a value between that of n_0 (air) and n_s (silicon). Including this interlayer in the system, it is possible to simply work out the effective reflection coefficients from the front side. This is the reflection from the first interface plus the reflection of the second interface.

In this first approximation, we do not consider the multiple reflections within the interlayer. We then plot the reflection coefficient of this example versus the refractive index of the interlayer.

In Figure 3.7 the blue line is the reference reflection without interlayer. The red line is the reflection with interlayer. The red curve has a minimum. This minimum is exactly at the value equal to the square root of the product of n_0 and n_2.

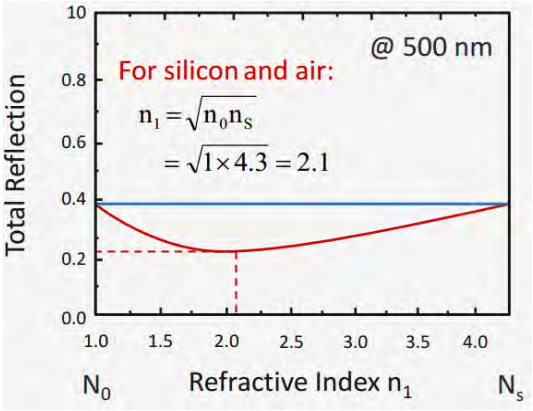

Figure 3.7 Reflection with and without the layer

In this example, by inclusion of a single interlayer, the reflection at the interface can be reduced from 38.8% down to 22.9%. Using more than one interlayer, also named refractive index grading, this reflection can be further reduced.

Another approach to anti-reflection is by using constructive and destructive interference of light. As I previously introduced, light can be considered as electromagnetic waves. Waves have the interesting properties that they can interfere with each other. Waves can be super imposed. So in the case of light the amplitude of the electric field of the wave A and B at certain position x,y,z at time t are super imposed. It means that the resulting amplitude of a wave A + B can be larger or smaller than the original waves A and

B. When two waves A and B are traveling in the same direction and are in phase, the resulting amplitude is larger than for a single wave. This situation is called “constructive interference”. When waves A and B are in antiphase, the amplitude of the resulting wave is equal to zero.This situation is called “destructive interference”. One can design an anti-reflection coating based on this principle. The green wave in Figure 3.8 shows the reflection back from the first interface and the red wave shows the wave which is reflected back from the second interface. If we look at the two waves coupled out of this system, they appear to be in antiphase. As a result the total amplitude of the electric field of the outgoing wave is smaller and the total irradiance coupled out of the system is smaller as well. The maximum destructive interference occurs when the product of the refractive index and thickness of the interlayer is equal to the wavelength divided by 4. In conclusion, the thickness is the wavelength divided by 4 times the refractive index of the coating.

$$d = \frac{\lambda}{4n_2} \tag{10}$$

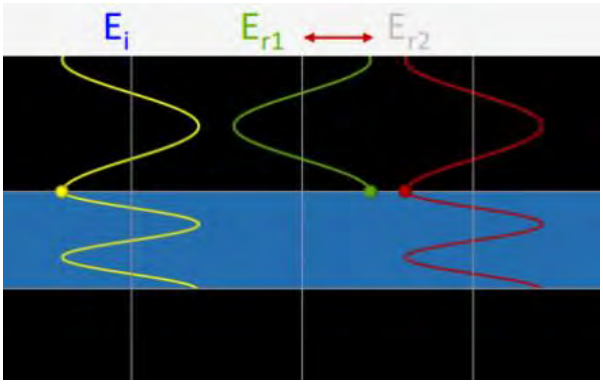

Figure 3.8 Destructive interference

Using an anti-reflection coating based on interference means that the typical length scale of the interlayer thickness must be in the order of the wavelength. A last and completely different approach for anti-reflection is the use of textured interfaces.

The length scale of the textured features is larger than the typical wavelength of light. The reflection and transmission of the light rays are determined by Fresnel's equations and Snell's law. The texturing helps to enhance the coupling of light into the layer. For example, for light that is perpendicular incident, light that is reflected at the textured surface, can be reflected at angles in which the trajectory of the light ray is incident somewhere else on the interface. Here part of the light will be transmitted into the layer and effectively less light will be reflected in reference to a flat interface.

To summarize, we have discussed three types of anti-reflection approaches, a Rayleigh film, anti-reflection coating based on destructive interference and enhanced coupling of light due to scattering at textured interfaces. If the absorber layer is not thick enough to absorb all the light, part of the light will be transmitted, Figure 3.4. As the absorption coefficients are larger in the blue spectral part, this usually plays a role in the red to infrared part of the solar spectrum. The light transmitted can be reflected back, which is a so-called back reflector. Some of the light can also be absorbed at the back contact. This can again be considered as a parasitic absorption loss.

In thin-film solar cells, where back reflectors and light scattering under angles start to play an important role, you would like to scatter the light back under the critical angle. Consider a single film of absorber material with a higher refractive index than its surroundings: the light is scattering between the two interfaces, down and up. In the ideal case, you would like to have all light trapped in the absorber layer, making the absorption path length so long that all the light is absorbed. Unfortunately, at every internal reflection part of the light is transmitted out of the film. However, this is not the case when there is a total internal reflection. From the Fresnel equations we know that above a critical angle the internal reflection becomes 100%. This means that if the light is scattered into the film above a critical angle, the light would be trapped. The critical angle is a function of the refractive index of both media.

If we consider silicon and air, this critical angle is rather small, 13.4°. However, absorber layers are usually confined between supporting layers. If we considered glass, with a refractive index of 1.5, the critical angle would become 20.4°. If we considered ZnO, a typical transparent conductive oxide, we would find a critical angle of 30.3 degrees.

4. Structure and properties of silicon

Crystalline silicon has the structure of a cubic diamond .The crystalline lattice indicates that atoms are arranged in a certain, repeated pattern. A crystalline lattice has long-range order and symmetry.

However, it does not mean that this pattern is the same in every direction, if we make a large cut through the lattice in fact, the various planes you can make do not look the same.

In Figure 4.1 we see two planes of two different cuts in a crystalline silicon lattice, which originally consisted out of three by three by three unit cells. We can see two surfaces: the first one is referred to as the (100) surface and the normal of this plane points in the (100) direction. The silicon at a (100) surface always has two back bonds and two other valence electronspointing to the front. The second surface is the (111) plane. It can be characterized by three silicon back bonds and one valence electron pointing in the normal to the plane.

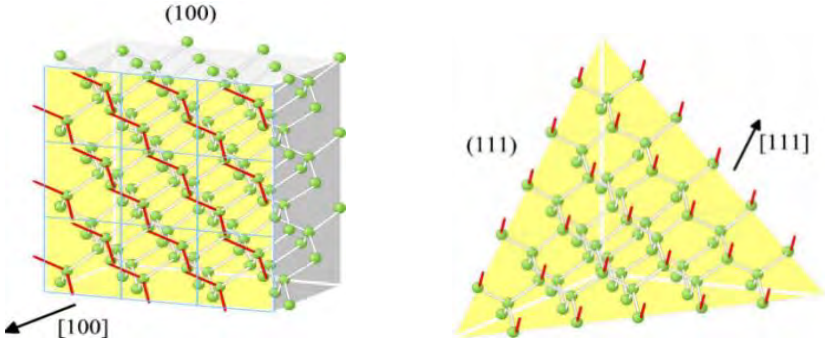

Figure 4.1 Different lattice plane

Why are these directions important? There are direct and indirect band gap materials. This can be expressed in the so-called electronic band dispersion diagram.

On the vertical axis you have the energy position of the valence and conduction band, and on the horizontal axis the crystal momentum, or the momentum of the charge carriers. To be excited into the conduction band, the charge carriers in an indirect band gap material require a change in energy and in momentum.

Figure 4.2 shows the real electronic band structure of the crystalline silicon. The white area reflects the energy levels in the forbidden band gap while the horizontal axis reflects the lattice momentum in various directions. The band gap of silicon is determined by the lowest energy point of the conduction band at X, related to the 100 direction, and the highest energy value of the valence band,at Γ.

The band gap energy is the difference between those two levels and equals 1.12 eV, or 1107 nm [1], expressed in wavelengths. This transition is an indirect transition. It's important to underline that the charge carriers need energy and momentum transfer to be excited. In Γ, crystalline silicon has a direct transition as well.

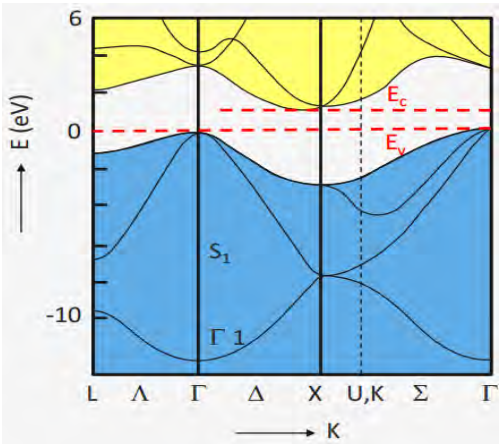

Figure 4.2 Real band gap of silicon

However, this transition has an energy of 3.4 eV, which equals a wavelength of 364 nm[1]. For an indirect band gap material it's less likely that a photon, above the band gap, is able to excite the electron into the conduction band in reference to a direct band gap material.

Recalling Figure 3.2 crystalline silicon is indicated by the red line, whereas GaAs and InP is indicated in yellow and green. This figure displays that in the visible spectrum crystalline silicon absorbs less than the GaAs and InP, but below 364 nm, it absorbs just as much as GaAs and InP, because silicon has a direct band to band transition here as well. Germanium, represented by the blue line, is like silicon: it is an indirect band gap material. It has a band gap of 0.67 eV, which means it already starts to absorb light at wavelengths below 850 nm[2]. In the visible part, germanium has some direct transitions as well.

4.1. Design rules of crystalline silicon

In this section I will describe several technical aspects which play an important role in the collection of the light excited charge carriers and the reduction of optical losses.

I have already introduced how an illuminated p-n junction can operate as a solar cell. Firstly it was used the simplification that both the p-doped and n-doped region have the same thickness. If we look at the c-Si technology, this is not the case in real devices. Let's look at the most conventional crystalline silicon solar cell. The solar cell is based on a p-type silicon wafer. The n-doped layer in the crystalline silicon PV technology is often called the emitter layer. This n-type emitter layer is much thinner than the wafer, the emitter has a thickness in the order of 1 micron. The remaining p-doped wafer can be in the order of 100 up to 300 microns. A large fraction of light is absorbed close to the front surface of the solar cell. In the first 10 microns most charge carriers are excited. By making the front emitter layer very thin, a large fraction of the light excited charge carriers generated by the incoming light is created within the diffusion length of the p-n junction. One of the processing methods to make the emitter layer is by solid state diffusion. The wafers are placed in a furnace, where the dopant atoms are present in atmosphere in the form of phosphine. These atoms react at these high temperatures with the surface. Furthermore, at such high temperatures the dopant atoms are mobile in the solid and based on Fick's law (10) the dopant atoms

will diffuse into the wafer. Similar for charge carrier diffusion, net diffusion occurs when there is a density gradient. The diffusion process is controlled such that the dopants penetrate into the solid to establish the desired emitter thickness.

$$J = -D\frac{\partial \phi}{\partial x} \quad (10)^{3} \qquad (10)$$

Another interesting topic concerns the way in which charge carriers in crystalline silicon solar cells are collected. Some of the crucial issues that play an important role in this charge collection include the emitter layer, the metal contacts and the back contact. At the p-n junction the light excited minority charge carriers are separated at the p-n junction. The minority electrons in the p-layer drift to the n-layer. These electrons have to be collected. Since the silicon n-emitter is not conductive enough it is necessary to use the more conductive metal contacts that will be placed on top of the emitter layer. When metal contacts are made of the cheap metal aluminum it means that the electrons have to diffuse laterally through the emitter layer to the contact to be collected. Let's quickly resume what the challenges for this transport of electrons to the contacts are.

First, we have mentioned the importance of the high lifetime of charge carriers. High lifetime in fact, guarantees large open-circuit voltages, so a better utilization of the band gap energy. This means that we have to reduce the recombination losses as much as possible.

In addition, recombination limits the collected current as well. Recombination in silicon occurs through both Shockley-Read-Hall and Auger recombination.

When considering Shockley-Read-Hall (SRH) recombination a bare c-Si surface contains many defects. The atoms on the silicon surface have some valence electrons which cannot make a molecular orbital with the absent neighboring atoms. These valence orbitals containing only one electron on the surface, act like defects, also called “dangling bonds”. The charge carriers can recombine defects through the SRH process. The probability and speed at which charge carriers can recombine is usually expressed in terms of the surface recombination velocity. Since a large fraction of the charge carriers is generated close to the front surface, a high surface recombination velocity at the emitter front surface will lead to charge carriers losses and consequently lower short-circuit current densities as well. The lifetime of the charge carriers is limited by the recombination processes at the wafer surface. In order to reduce the surface recombination, two approaches are used.

The first is based on reducing the number of defects at the surface. This can be achieved by putting a thin layer of a different material on top of the surface. It will in fact partially restore the bonding environment of the silicon atoms. More in specific, the material must be an insulator and it must force the electrons to remain in and move through the emitter layer.

The typical chemical passivation layers that are being used on emitter layers are: silicon oxide and silicon nitride. Silicon oxide layers are formed by heating up the silicon surface in an oxygen-rich atmosphere. The surface oxidizes resulting in a thin layer of silicon oxide. SiN can be deposited using plasma-

[3] is the "diffusion flux" [(amount of substance) per unit area per unit time], for example

D is the diffusion coefficient or diffusivity in dimensions of [length2 time−1], for

enhanced chemical vapor deposition. That process technology is more related with thin-film PV technologies.

A second approach to reduce the surface recombination velocity is to reduce the minority charge carrier density near the surface. As the surface recombination velocity is limited by the minority charge carriers, a low as possible minority charge carrier density at the surface region would be beneficial. It means that with increasing the doping of the emitter layer, we decrease the density of the minority charge carriers. This results in a lower recombination velocity at the surface. However, this is again in competition with the diffusion length of the minority charge carriers.

It is important to note that many charge carriers are generated by the blue-ish photons close to the surface. To utilize these light excited minority charge carriers, the diffusion length of the holes has to be large enough to reach the depletion zone at the p-n junctions. Increasing doping levels, the diffusion length of the minority holes in the emitter layer decreases. Therefore, too high doping levels or too thick emitter layers would result in a poor blue response or low External Quantum Efficiency (EQE) values in the blue part of the solar spectrum. Such layer could be referred to as a "dead layer" as the light excited minority charge carriers can not be collected.

Analyzing in more detail the metal-emitter interface we cannot use an insulating passivation layer, like SiOx or SiN anymore since we need electrons to conduct from the semiconductor to the metal. This means that the metal-semiconductor interface has more defects and therefore an unwelcome high interface recombination velocity. In addition a metal-semiconductor material induces a barrier for the majority charge carriers. Notice that higher barrier will give rise to a higher contact resistance. Again high doping levels can reduce the recombination velocity at the metal-semiconductor interface and reduce the contact resistance. As a consequence the area of the interface between the metal and the semiconductor should be reduced in order to minimize the recombination at the interface defects as much as possible, and to have the emitter directly under the contact as heavily doped as possible. This higher doped region in is indicated by N+. In the Figure 4.1.1 the contact area between metal and interface is kept as small as possible and the sides of the metal contacts are buried in the insulating passivation layer. The area below the contact has been heavily doped. These two approaches reduce the recombination and collection losses at the metal contact. The classic metal grid pattern on top of a solar cell looks like a grid. It is the road map for the electrons.

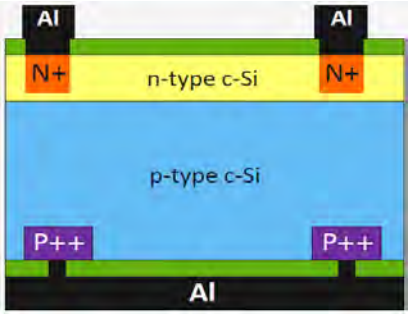

Figure 4.1.1 Front and back contacts

The larger contacts are called “busbars”. The smaller country roads going from the busbar to the edge of the solar cell, are called 'fingers'. Firstly, fingers have a resistance which is indicated with R. If L is the

length of the finger, W its width and H its the height and if ρ is the electrical resistivity of the metal, we can describe the resistance R as ρ times length divided by the height and the width. The equation shows that the longer the path length for an electron is, the larger the resistance the electron experiences. In addition, the smaller the cross-section (width times height) of the finger, the larger the resistance will be. It is important to note that the resistance of the contacts will act as a series resistance in the equivalent electric circuit. Larger series resistance will result in lower fill factors of the solar cell. Hence the best condition is to have the finger cross-section as large as possible. Since the n-type silicon has a higher resistivity as the metal, the charge carriers in the emitter layer also experience a resistance. As the metal contacts are at the front surface, they act as an unwelcome shading object, because light incident on the front contact area cannot be absorbed in the PV active layers.

In brief the preference of keeping the contact area as small as possible is in contrast with the preference to have a large as possible cross-section (more specifically the contrast is about a small as possible width and a high as possible height).

Therefore we count several effects in competition with each other. Let's look for a moment at the relation between losses and the finger spacing. With increasing finger spacing the power losses of the solar cell decreases due to shading. In contrast, the losses due to the resistivity in the emitter layer and the metal fingers increases. This means that the total loss has a minimum Figure 6.1.

Similar plots can be made for the width of the contact. The larger the width, the larger the losses due to shading. The resistive losses in the metal fingers decrease with the increase of finger width. Again there exists a width, which has a minimum loss. Optimizing the front contact pattern is therefore a complex interplay between the finger width and spacing.

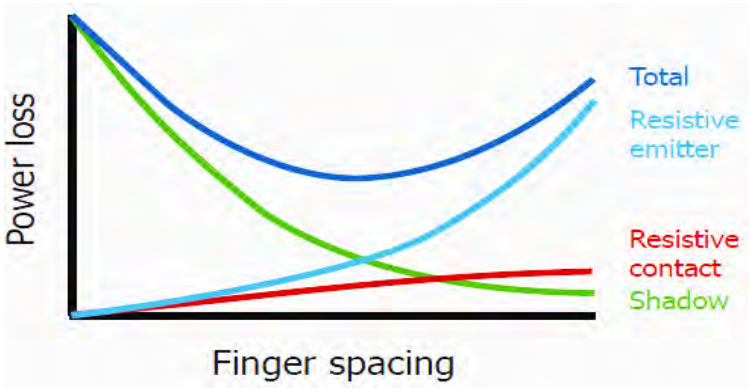

Figure 4.1.2 Power loss as a function of ginger spacing

At the back surface of the solar cell we can detect similar issues. As the electrons have to be collected in the n-type layer, the holes are collected at the back contact. As electrons are the only charge carriers that exist in the metal, the holes recombine with the electrons at the contact interface. If the distance between the p-n interface and the back contact is smaller than the typical diffusion length of the minority electrons, the latter can be lost at the defects at the back contact interface due to the SRH recombination. To reduce this loss mechanism first, we can reduce again the area between the metal contact and the semiconductor. It is possible to make point contacts while the rest of the rear surface is then passivated by an insulating passivation layer, similar as the one we have discussed for the cases of the emitter front surface.

The loss mechanism of recombination of electrons at the back contact can be further reduced by a so-called back surface field. A higher p-doped region is placed above the point contacts at the rear surface, indicated by P++. Moreover an interesting question concerns the functioning of a back surface field.

For the moment we have put the solar cell on its side. Below the solar cell you see the band diagram indicating the various interfaces. The interface between the lower-doped p-region and the higher-doped p-region acts like a p-n junction. In this case it will act as a barrier for the light excited minority electrons in the lower-doped region to diffuse to the back surface. The space charge field behaves like a "defects at the back contact interface passivation" and allows to have higher levels for the electron minority density in the p-doped bulk.

The previous paragraphs were mainly focused on the topic of managing the charge carriers whereas the following part will develop the discussion about the management of the photons in a crystalline silicon solar cell device.

The optical loss mechanisms are: shading, reflection losses, parasitic absorption losses in the non-PV active layers, and light that is not absorbed in the silicon layers but is lost at the back contact.

Shading losses are caused by the front contact grid as I mentioned earlier. The optimum contact grid at the front is the result of the competition between reduction of the shading losses and a reduction of the resistivity losses in the metal contact and the emitter layer. Secondly, the reflection at the front surface can be considered as a loss mechanism.

Methods to reduce these losses have long been debated. The first one was based on the Rayleigh film principle: by putting a film with a refractive index smaller than that of silicon wafer between air and the wafer, you can reduce the losses. The optimum value for the refractive index of the intermediate layer equals the square root of the product of refractive indices of the two other media. For silicon and air at 500 nm this leads to an optimum refractive index of 2.1.

Note, that in practice a solar cell is encapsulated under a glass plate. The glass plate will be beneficial to refractive index grading as well, reducing the reflection losses further. Secondly, while using the concept of destructive interference we can choose the thickness and refractive index of an anti-reflection coating; by doing so, in a certain wavelength the irradiance coupled out of solar cell is minimized. The light reflected from the front surface is in anti-phase with the light reflected from the back surface.

The thickness of such layer should be the wavelength divided by 4 times the refractive index. If we consider a welcome reflective index of 2.1 we can obtain for light of 500 nm at an optimal thickness of 60 nm for an anti-reflection based on destructive interference.

As I previously introduced, one of the typical passivation layers of standard crystalline silicon is silicon nitride. A multicrystalline silicon wafer without the SiNx layer is represented in Figure 6.1 . A lot of light is reflected by the wafer and next to it it is shown a multicrystalline silicon with a silicon nitride passivation layer. In the image much less light is being reflected.

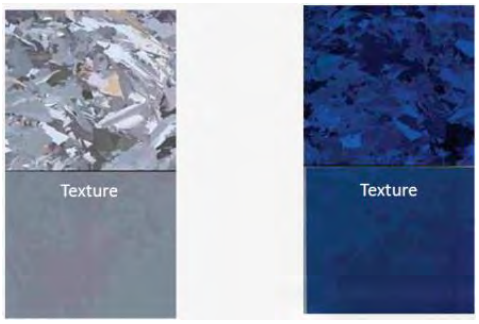

Figure 4.1.3 Antireflective layers

Interestingly, the refractive index of SiN is in the range of 2 up to 2.2 at 500 nm, close to the optimum for refractive index grading. Typical thicknesses are in the same range as the 60 nm discussed earlier. Note, that the surface of the solar cell looks a bit blue-ish. This shows that the reflection of blue light by the SiNx is larger than for the other wavelengths. As discussed before, texturing of the surface can improve the light incoupling as well.

4.2. High efficiency concepts of c-Si wafer

In this block three examples of highly efficient solar cells based on crystalline silicon wafers are considered. As discussed in previous sections, various types of wafers with different qualities of silicon exist. To achieve the highest efficiencies, the bulk recombination must be as low as possible. Therefore the high-efficiency crystalline silicon solar cells are based on monocrystalline wafers.

The first high-efficiency crystalline silicon solar cell was developed by Martin Green's group at the University of New South Wales in the late 80s and the early 90s. He developed the PERL concept, (Passivated Emitter Rear Locally diffused) which uses a p-type float-zone silicon wafer and that is the “father” of many other PV technologies developed afterwards. This innovative concept has approached a conversion efficiency of 25%.

The optical losses of the PERL solar cell at the front side are minimized using three important characteristics.

First, the top surface of the solar cell is textured using inverted pyramid structures. This microscopic texture allows a fraction of the reflected light to be incident on the front surface for a second time. This enhances the total amount of light coupled into the solar cell.

Secondly, the inverted pyramid structures are covered by a double-layer anti-reflection coating (ARC) which results in an extremely low top surface reflection. A double-layer coating of magnesium fluoride and zinc sulfide is often used as an antireflection coating.

Thirdly, the contact area at the front side has to be as small as possible, to reduce the shading losses.

In the PERL concept these very thin and fine metal fingers are processed using photolithography[4] technology. The emitter layer is smartly designed and should be highly doped underneath the contacts, which in the PERL concept is achieved by heavily phosphorous diffused regions. The rest of the emitter is moderately doped, or lightly diffused, to preserve an excellent "blue response". The emitter is passivated with an silicon oxide layer on top of the emitter to suppress the surface recombination velocity as much as possible. The surface recombination velocity has been suppressed to the level that the open-circuit voltages with values of above 700 mV have been obtained using the PERL concept. At the rear surface of the solar cell, point contacts have been used in combination with thermal oxide passivation layers. The oxide operates as a passivation layer of the non-contacted area, to reduce the unwelcome surface recombination. A highly doped boron region, created by local boron diffusion, operates as a local back surface field, to limit the recombination of the minority electrons at the metal contact.

On the other hand the PERL concept previously described includes some expensive processing steps. The Chinese Suntech company developed in collaboration with the University of New South Wales a more commercially viable crystalline silicon wafer technology, which is inspired on the PERL cell configuration.

A second successful cell concept which is commercialized by SunPower is the interdigitated back contact (IBC) solar cell. The principle of interdigitated back contact concepts is that it does not suffer from shading losses of a front metal contact grid. All the contacts responsible for collecting of charge carriers at the n- and p-side are positioned at the back of the crystalline wafer solar cell. An advantage of these interdigitated concepts are that you are able to use monocrystalline float-zone n-type wafers. The n-type wafers have some advantages above p-type wafers.

First, the n-type wafers do not suffer from light-induced degradation. In p-type wafers simultaneously boron and oxygen are present, which under light exposure start to make complexes that act like defects. The light-induced degradation causes a reduction of the power output with 2-3% after the first week of installation. This effect is not present in n-type wafers.

The second advantage is that n-type silicon is not that sensitive for impurities like for instance iron impurities. As a result less efforts have to be made to make a high electronic quality of n-type silicon, meaning that high-quality n-type silicon can be processed cheaper than p-type.

On the other hand, p-doped wafers have the advantage that the boron doping is more homogeneously distributed over the wafer as for n-type. This means that within one n-type wafer the electrical properties can vary within the same wafer. This effect lowers again the yield of solar cell production based on n-type monocrystalline wafers. Back contacted solar cells use, in contrast to the PERL concept, n-type float-zone monocrystalline silicon wafers. An interdigitated back contact is lacking one large p-n junction. Instead the cell has many localized junctions. The holes are separated at a junction

[4]Photolithography is a process used in microfabrication to pattern parts of a thin film or the bulk of a substrate. It uses light to transfer a geometric pattern from a photomask to a light-sensitive chemical "photoresist", or simply "resist," on the substrate. A series of chemical treatments then either engraves the exposure pattern into, or enables deposition of a new material in the desired pattern upon, the material underneath the photo resist. For example, in complex integrated circuits, a modern CMOS wafer will go through the photolithographic cycle up to 50 times.

of p+ and the n-type silicon, whereas the electrons are collected using a n+ type silicon. The semiconductor-metal interface is kept as small as possible to reduce the unwelcome recombination at this defect-rich interface. Another advantage is that the cross-section of the metal fingers can be made much larger to reduce the resistive losses of the contacts as much as possible. The fact that the contacts do not cause any shading losses at the back, allows them to become larger. The passivation layer can have a low refractive index such that it operates like a backside mirror. It will reflect the light above 900 nm, which is not absorbed during the first pass, back into the absorber layer, enhancing the absorption path length.

An interdigitated back contact solar cell would look like the one in Figure 4.2.1. At the back you have two metal grids. One collects the current of the n-type contacts and the other collects the current of the p-type contacts.

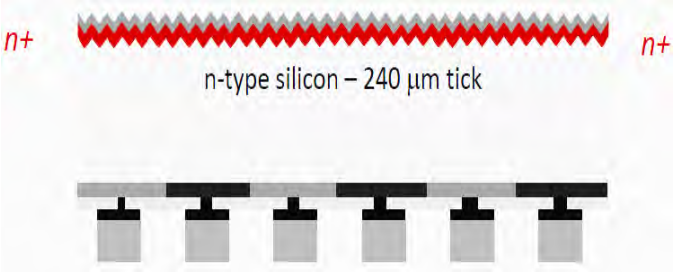

Figure 4.2.1 Interdigitated back contact solar cell

At the front side the losses of the light excited charge carriers due to surface recombination is suppressed by using the same tricks like the back surface field as discussed for the rear surface for solar cells, based on p-type wafers. The surface recombination velocity of the front surface is determined by the minority charge carriers, in this case, the electrons.

Consequently, we have to create a front surface field. A higher n-doped region is placed at the front surface indicated by n+. The interface between the higher-doped n-region and the lower-doped n-region acts again like a p-n junction. In this case it will act as a barrier for the light-excited minority holes in the lower doped region to diffuse to the front surface. The front surface field behaves like a passivation of the defects at the front interface and allows to have higher levels for the hole minority densities in the p-doped bulk. At the front side the reflective losses can be reduced using the same tricks as discussed for the PERL solar cell. Deposition of double-layered anti-reflection coatings and texturing of the front surfaces. SunPower is the company that has developed a cell technology based on interdigitated back contacts, and they have achieved high solar cell efficiencies of 24.2%.

5. Heterojunction solar cells

An alternative concept with high efficiencies is the so-called crystalline wafer based heterojunction solar cells. So far it has been introduced the concept of p-n junctions with a depletion zone. These junctions are fabricated by different doping types within the same semiconductor material. This means the band gap in the p- and n-doped material is the same. Such p-n junction is called a homojunction. However, you can also make a junction by two different semiconductor materials. For instance one semiconductor material that is p-doped and another type of semiconductor material that is n-doped. This is what we call a heterojunction. In the c-Si wafer based heterojunction we make use of two types of silicon based semiconductor materials. One is again a n-type float zone monocrystalline silicon wafer, the other material is hydrogenated amorphous silicon. This is a silicon material in which the atoms are not ordered in a crystalline lattice but in a disordered lattice. This material has a higher band gap than the one of crystalline silicon. Moreover, amorphous silicon can be n-doped and p-doped as well, using phosphorous or boron. In Figure 5.1 the band diagram of a heterojunction cell is shown.

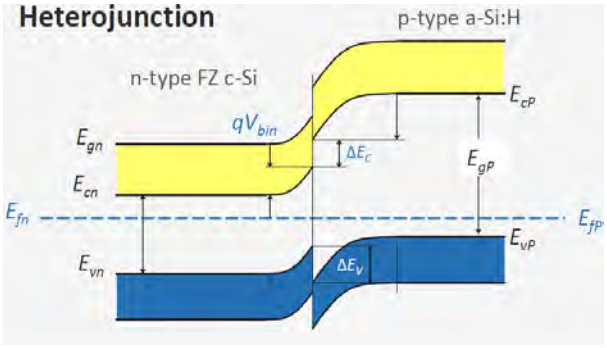

Figure 5.1 Band diagram of a heterojunction cell

Figure 5.1 the Band diagram of a heterojunction cell in dark and thermal equilibrium Next to the induced field due to the space charge region, some local energy steps are introduced. These steps are caused by the fact that both band gaps are not the same. At the junction which is displayed in the image the valence band is higher positioned in the p-type amorphous silicon in reference to the n-type crystalline silicon. This will allow the minority charge carriers, the holes, to drift to the p-type silicon. However, in this example the holes experience a smaller barrier. A large fraction of the holes can move through this barrier and this phenomena is called tunneling.

The crystalline silicon wafer based heterojunction solar cell is a concept which has been invented by the Japanese company Sanyo, which is currently part of Panasonic. The Panasonic cell is called the HIT cell, which stands for “heterostructure with intrinsic thin film”.

The HIT cell configuration has two junctions. The junction at the front side is formed using a thin layer of only 5 nanometers of intrinsic amorphous silicon, which is indicated by the red color in Figure 5.2. A thin layer of p-doped amorphous silicon is deposited on top and here is indicated with the blue color. The heterojunction forces the holes to drift to the p-layer. At the rear surface a similar junction is made. First,

a thin layer of intrinsic amorphous silicon is deposited on the wafer surface. On top of the intrinsic layer an n-doped amorphous silicon is deposited.

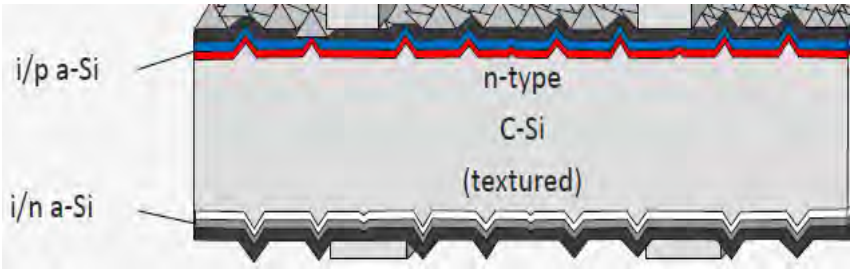

Figure 5.2 HIT cell structure

As discussed earlier, for high-quality wafers, like this n-type float-zone monocrystalline silicon wafer, the recombination of charge carriers at the surface determines the lifetime of the charge carriers. The advantage of the HIT concept is that the amorphous silicon acts like a very good passivation material. In this approach the highest possible lifetimes for charge carriers are accomplished. The c-Si wafer based heterojunction solar cell has the highest achieved open-circuit voltages among the crystalline silicon technologies. Panasonic achieved an open-circuit voltage of 750 mV. The conductive properties of the p-doped amorphous silicon are relatively poor.

In homojunction solar cells, the diffusion to the contacts takes place in the emitter layer. In contrast, in a HIT solar cell this occurs through the transparent conductive oxide material, like an ITO, which is deposited on top of the p-doped layer. The ITO is needed as the conductivity of the p-type layer is too poor. This results in such small diffusion lengths that a practical metal finger spacing can not be achieved using the p-type layers. Therefore ITO is used. An advantage of the HIT cell concept is that it allows to introduce the same contact scheme at the n-type back side. It means that this solar cell can be used in a bifacial configuration, it can collect light from the front, and scatter and diffuse light falling on the backside of the solar cell. Another important advantage of the HIT solar cell is that the amorphous silicon layers are deposited using cheap and straightforward plasma-enhanced chemical vapor deposition technology at low temperatures, not higher than 200 degrees Celsius. In sum, it means that making the front surface and back surface field in this type of solar cells is very cheap.

Furthermore, this technology allows to use the n-type wafers. Summarized, the high-efficiency crystalline silicon wafer based solar cells are described as follows: the record efficiency of a PERL solar cell was 25%, however, this was a lab-scale solar cell with an area of 4 cm^2. The record efficiency for an interdigitated crystalline silicon solar cell has been achieved by SunPower. They achieved an efficiency of 24.2 % on a wafer size of 155 cm^2. Finally, for the c-Si wafer based heterojunction solar cell, Panosonic achieved an efficiency of 24.7% on a wafer size of 102 cm^2.

The efficiencies for multicrystalline silicon solar cells are lower as the wafer quality is lower. The best efficiency achieved is 19.5% by Q-cells on a wafer with a size of 243 cm^2. This is around 5% absolute below the record efficiencies based on monocrystalline silicon wafers

6. III-V PV Technology

The dominant PV technology in the current market is PV technology based on c-Si wafers. Probably this technology will remain the dominant PV technology in the market for a long time.

In this section I will draw the description of the alternative PV technologies like the thin-film technologies, also referred to as the second generation PV technology. This section will be just a general introduction into the various PV technologies, focusing on the working principles of the various devices, the current status and the future challenges of the various technologies.

I would like to start with the III-V PV technology. This is the solar cell technology which results in the highest conversion efficiencies under both 1 sun standard test conditions and concentrated sun conditions. It is mainly used in space technology and in concentrator technology. As some concepts use crystalline germanium and GaAs (Gallium Arsenide)wafer as substrate, it might not be a real thin-film PV technology, like thin-film silicon, CdTe (Cadmium Tellurid) , CIGS (Copper Indium Gallium Selenide) or organics, which will discuss later in this work, however, the III-V based absorber layers itself can be considered as thin in reference to the crystalline silicon wafers. The III-V materials are based on III-valence electron elements like aluminum, gallium and indium and the V-valence electron materials as phosphorous and arsenic. Various different semiconductor materials such as gallium arsenide, gallium phosphide, indium phosphide, indium arsenide, and more complex alloys like GaInAs, GaInP, AlGaInAs and AlGaInP have been explored.

I would in this section briefly focus on the standard GaAs semiconductor material. Its lattice has a tetrahedral diamond lattice structure just like silicon. However, every gallium atom neighbors four arsenicum atoms, and every arsenic atom neighbors four gallium atoms. Compared to silicon it has a slightly larger lattice constant, and is significantly heavier than silicon. Both gallium and arsenic are roughly twice as heavy as silicon. In Figure 6.0 we see the electronic band dispersion diagram again. We can easily see that the band gap of GaAs is a direct band gap material.

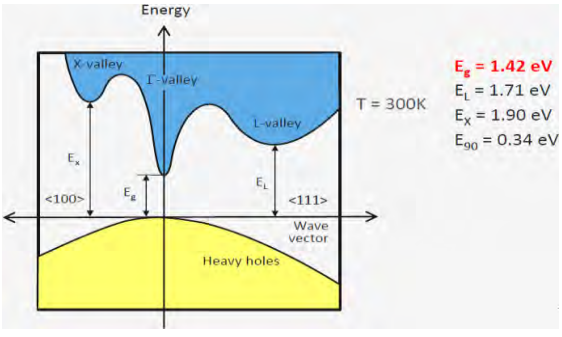

Figure 6.0 Direct band gap of GaAs

The highest energy level in the valence band is vertically aligned with the lowest energy in the conduction band. It means that only transfer of energy is required to excite an electron from the valence to the conduction band. No transfer of momentum is required. The direct band gap transition is around 1.42

eV, which is the band gap of GaAs. Here we see again at the absorption coefficient versus the wavelength. As you can see here, the absorption coefficient of GaAs is significantly larger than for silicon [2], [3].

As example I also show the III-V material, InP. It means that to absorb the same amount of light in reference to a silicon wafer, the thickness of the GaAs film can be more than an order of magnitude thinner. Another advantage of the direct III-V semiconductor materials shown here is that the band gap is relatively sharp. The absorption coefficient increases quickly above the band gap energy. If we look at the utilization of the band gap energy, due to the direct band gap properties, radiative recombination processes can become an important recombination mechanism as well. The Shockley-Read-Hall recombination can be kept low as the typical epitaxy processes used to deposited III-V films, results in high purity films.

Why does the III-V technology result in high conversion efficiencies? The III-V technology PV devices are based on the multi-junction concept. More than one band gap material is used. As I previously introduced, by using only one single band gap material, the theoretical efficiency is limited by the Shockley-Queisser limit. Either a large fraction of the energy of the energetic photons are lost as heat, or the photons below the band gap are lost as they are not absorbed. A large fraction of the energy carried by the photons is not used. However, if we use more band gaps, you see that the same amount of photons can be used, and less energy is wasted as heat. Consequently, simultaneously large parts of the solar spectrum and large parts of the energy in the solar spectrum can be utilized by using more than one p-n junction. It is based on a low band gap material, a germanium substrate wafer. Note, that germanium has a band gap of 0.67 eV. The middle cell is based on GaAs and has a band gap of 1.4 eV [2], [3]. The cell at the top is based on GaInP2 with a band gap in the order of 1.86 eV[2],[3].

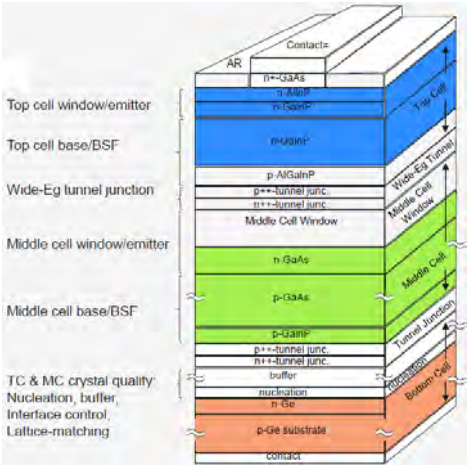

Figure 6.1 Multi-junction solar cell

The p-n junction at the window layer at which the solar light enters the PV device is called the top cell. As the spectral part with the most energetic photons like blue light has the smallest penetration depth in materials, the high band gap junction always acts like the top cell. As the near infrared light outside the visible spectrum has the largest penetration depth, the bottom cell is the cell with the lowest band gap. This cell has to harvest the photons from spectral parts with the lower energetic photons. In Figure 6.2 it is possible to see the J-V curve of three single p-n junctions.

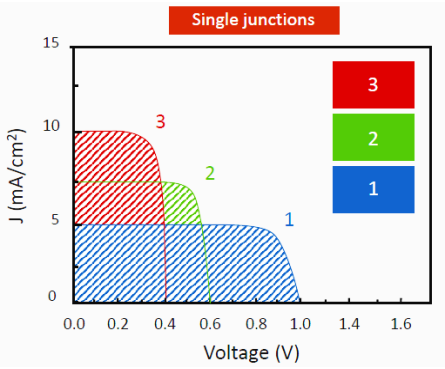

Figure 6.2 J-V curve of three single p-n junction

P-n junction 1 has the highest open-circuit voltage and the lowest short-circuit current density, this means this p-n junction has the highest band gap. P-n junction 3 has a low open-circuit voltage and a high current density, consequently it has the lowest band gap. P-n junction 2 has a band gap in between. If we would like to make a triple junction out of these three p-n junctions, p-n junction 1 will act as the top cell, p-n junction 2 will act as the middle cell and p-n junction 3 will act as the bottom cell. What would the J-V curve of a triple-junction look like? First we will consider the equivalent electric circuit.

Figure 6.3 shows the equivalent electric circuit of an ideal single junction solar cell.

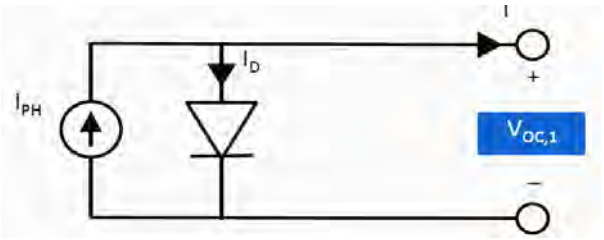

Figure 6.3 Ideal junction equivalent circuit

Every p-n junction in a multi-junction solar cell can be represented by this circuit. However, it is necessary to understand how will these solar cell circuits are connected in the representative multi-junction circuit. In a parallel circuit the voltage over all solar cells is equal and the currents do add up. However, the various solar cells have different band gaps and therefore different open circuit voltages going from high voltage for the top cell down to a low voltage for the bottom cell. Secondly, the current density generated in all cells has to conduct through all three cells to be collected at the front and back contacts. As a result the multi-junction can be interpreted as a series connection of single junction solar cells. Now we return to the question: How does the J-V curve of the triple junction look like? The voltages of the individual cells add up in the triple junction like in a series connection. The current density in a series connection is equal over the entire solar cell. This means that the current density is determined by the p-n junction generating the lowest current. The resulting J-V curves look like Figure 6.4.

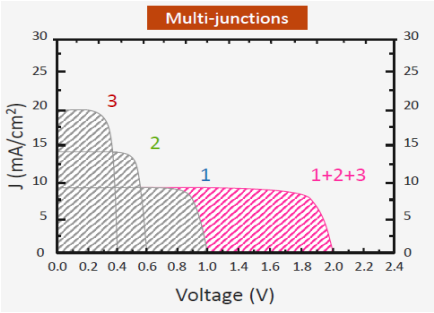

Figure 6.4 J-V curve of triple junction

The voltages add up and the current is determined by the cell delivering the lowest current.

If we place three p-n junctions in series it means that the p-layer of for instance the top cell and the n-layer of the middle cell form a p-n junction as well. This p-n junction is in the reverse direction compared to the p-n junction forming the three single junction solar cells. This would significantly lower the voltage of the total triple junction. The creation of such reverse junction can be prevented by the inclusion of a so-called tunnel junction Figure 6.5.

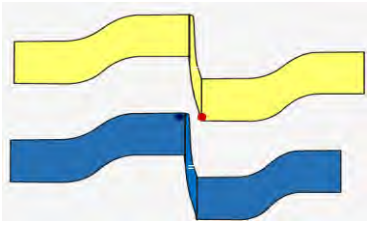

Figure 6.5 Tunnel junction band gap

The high band gap tunnel junction is relative thin. It means that the valence band at one side is lined up with the conduction band at the other side of the tunnel junction. The depletion zone of such junction is extremely narrow. As a result the slope of the valence band and conduction band are so steep that the electrons from n-layer tunnel through the small barrier to the p-layer, where they recombine with the holes. Important is that the resistance of the tunnel junction is low resulting in a low voltage loss over the tunnel junction. Looking at a triple junction, it means that the holes in the p-layer of the top cell have to recombine with the electrons of the n-layer of the middle cell. The holes in the p-layer of the middle cell have to recombine with the electrons of the n-layer of the bottom cell Figure 6.6.

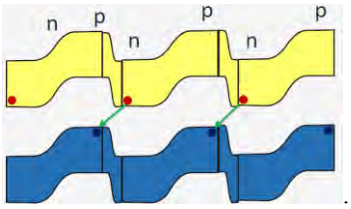

Figure 6.6 Recombination in a multi-junction cell

The electrons of the top cell are collected at the front contact and the holes in the p-layer at the back contact. This demonstrates that the recombination current at the tunnel junctions represent the current density of the triple junction. The cell producing the lowest current will determine the current density of the cell, just like we expected for a series connected cells.

7. Perovskite solar cells

Perovskite solar cells based on organometal halides represent an emerging photovoltaic technology. These solar cells stem from dye-sensitized solar cells. Perovskite is the term for a particular mineral crystal structure, most commonly a calcium titanium trioxide mineral, and is applied to anything that adopts this same structure.

The first discovered liquid-based dye-sensitized solar cells structure in 2009, produces a photocurrent with a power conversion efficiency (PCE) of around 3-4%. The PCE was doubled after 2 years by optimizing the perovskite coating conditions. However, the liquid-based perovskite solar cell receives little attention because of its stability issues, including instant dissolution of the perovskite in a liquid electrolyte. Its high efficiency, almost 10%, perovskite solar cell was achieved in 2012 by substituting the solid hole conductor with a liquid electrolyte, rised quickly to 18% just in 2 years.

As a matter of fact perovskite solar cells are a promising photovoltaic technology since PCE values over 20% are realistically anticipated with the use of cheap organometal halide perovskite materials. Therefore, in this section the opto-electronic properties of perovskite materials and recent progresses in perovskite solar cells are described. Russian mineralogist L.A. Perovski, who gave the name to the mineral, has a specific crystal structure with the ABX_3 formula (X = oxygen, halo- gen). The larger A cation occupies a cubo-octahedral site shared with twelve X anions while the smaller B cation is stabilized in an octahedral site shared with six X anions illustrated in Figure 7.1. The most studied perovskites are oxides due to their electrical properties of ferroelectricity or superconductivity.

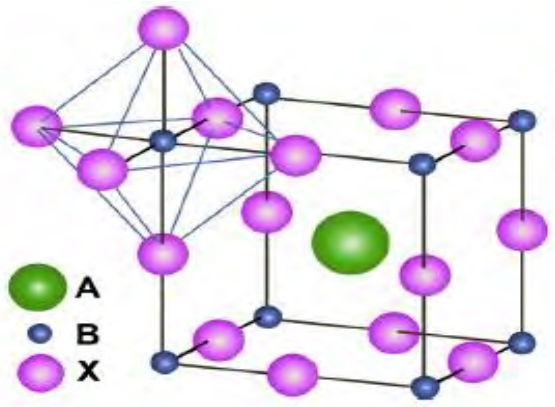

Figure 7.1 structure of Perovskite material

There weren't many extensive studies regarding halide perovskites until layered organometal halide perovskites had stepped forward to exhibit a semiconductor-to-metal transition with increasing dimensionality. Beside changes in electrical properties, the band gap decreased with increased dimensionality from 2D to 3D. A narrow band gap is beneficial for solar cell applications. Miyasaka applied 3D perovskite CH3NH3PbX3 (X = Br, I) as an inorganic sensitizer in dye-sensitized solar cells in 2009. They demonstrated a power conversion efficiency (PCE) of 3.1% for X = Br and 3.8% for X = I.

Park et al. reported PCE of 6.5% using CH3NH3PbI3. At the given TiO2 film thickness of about 3.6 mm, CH3MH3PbI3 perovskite showed an absorption coefficient that was 10 times greater than that of the conventional ruthenium-based molecular dye. Organolead halide, which is ionic crystal, perovskite is not suitable for liquid electrolyte-based sensitized solar cells because of stability concerns. This instability problem was solved by substituting a solid hole conductor for the liquid electrolyte. Park et al. first reported long-term stable perovskite solar cells with PCE as high as 9.7% .

Rapid progress was made over the years, and PCEs exceeding 15% was achieved using organolead halide perovskite. Perovskite solar cell technology was selected as one of the biggest scientific breakthroughs of 2013. Figure 7.2 displays the progress of different techniques and also perovskite's ascent.

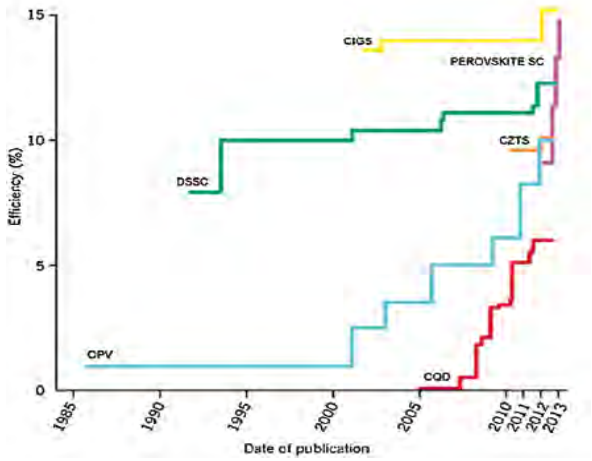

Figure 7.2 The progress of different techniques for solar applications

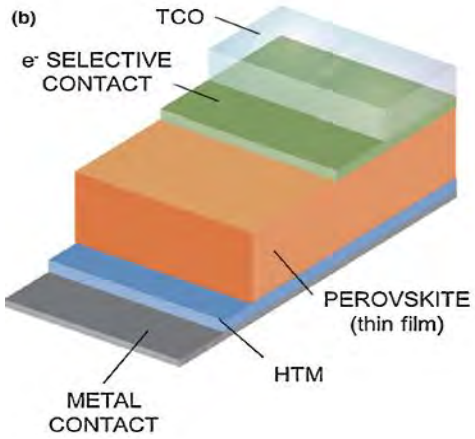

Figure 7.3 Perovskite solar cell structure. TCO: transparent conducting oxide; HTM: hole transport material

7.1. Structure of perovskite material

Perovskite materials have similar crystal structures to $CaTiO_3$ and can be represented by the simple building block ABX_3, where B is the metal cation and X is an oxide or halide anion. In the case of the organolead halide perovskite, the smaller lead cations (Pb_2+) are surrounded by six halide anions (I−) at the corners, forming six-fold coordinated octahedrons that extend to a three-dimensional network by connecting the corners. The larger cationic alkylammonium (CH_3NH_3+) groups balance the charge between the octahedron layers. The stability and the distortion of the perovskite structure are dependent on the tolerance factor t. Geometric tolerance factor *t* is defined to estimate the formability of perovskite.

$$t = \frac{r_A + r_X}{\sqrt{2}(r_B + r_X)} \quad (12)$$

Where r_A, r_B and r_X are the effective ionic radii for A, B, X respectively of the general perovskite's formula ABX_3.[4] An ideal cubic perovskite is expected when t=1while for t<1 octahedral distortion is expected. Furthermore the symmetry is compromised for t<1 which may affect electronic, optical and dielectric properties. For alkali metal halide perovskite, formability is expected for 0.813 < t < 1.107[4]–[6].

Initially the perovskite solar cells were fabricated using the configuration of mesoscopic dye-sensitized solar cells (DSSC) in which perovskites nanocrystals were used as the light absorber in lieu of the dye in a liquid electrolyte-based device. Progressively, deposition of nanocrystals ($CH_3NH_3PbI_3$) onto mesopurous TiO_2 films was improved, resulting in a electrolyte cells. However, due to rapid decomposition of the organolead halide perovskite in electrolyte, performance of this cells degrade in few minutes. This technique had a PCE of 9.7%. at the same time was emerging a new p-type material named poly-triarylamine (PTAA) as a suitable hole transmission material HTM for perovskite-sensitized solar cells.

PTAA lead up to 12% the efficiency of this cells. HTM for perovskite solar cells must have a high hole mobility, which could reduce series resistance and rise fill factor of the cells. Even though one-step deposition of perovskite nanocrystals was used in the beginning its performance was low. Therefore, this is the reason that made one-step deposition uncomfortable. The problem was overcome using the sequential deposition method.

First of all PbI_2 was deposited on TiO_2 films and by chemical reaction with CH_3NH_3I converted itself into the perovskite. By using the Two-step deposition approach for cells production, performance rises up to 15%, which is a considerable step forward for the fabrication of high-performance perovskite solar cells.

In the case of the classic sensitized solar cell, excited electrons are transferred into the TiO_2 mesoporous layer and then diffuse to the compact TiO_2/transparent conducting oxide (TCO) anode. A significant fraction of the electron transport could occur through the organolead perovskite phase itself because perovskites are significantly more conducting than TiO_2. The electron mobility μ of TiO_2 is about 7,5[cm^2/V*s] which is 3-4 times less than perovskite material's mobility, that is 25 [cm^2/V*s][3], recalling organolead halide perovskites that satisfy the three prerequisites for a well-performing cell.

Otherwise, they have strong light absorption, a high carrier generation ability and excellent electron and transport proprieties.

Since organolead halide perovskites are more conductive (10^{-3} S/cm) than the HTMs currently used, high-efficiency perovskite solar cells require a capping layer of HTM to prevent contact between the perovskite and metal cathode. However, this increases the series resistance and decreases the fill factor of the resulting cells, which limits the device performance. Another strategy for the development of high-performance perovskite solar cells is to develop multi-junction tandem devices, where there is a top subcell with a wider band gap to absorb the high-energy photons while the low-energy photons pass through the top subcell and are absorbed by the bottom subcell that has a narrower band gap semiconductor. The organolead halide perovskite band gap can be included between 1,5 and 2,2 eV by tailoring its chemical species. This makes them suitable for use as top subcell. They will match with crystalline silicon that has a band gap of 1,1 eV.

8. Status and prospect of solar energy

First I would like to discuss the production of solar modules. In Figure 8.1 is shown the worldwide solar cell production. The vertical axis represents the annual production. Annual production is expressed in the total produced power capacity in MW. The horizontal axis represents time.

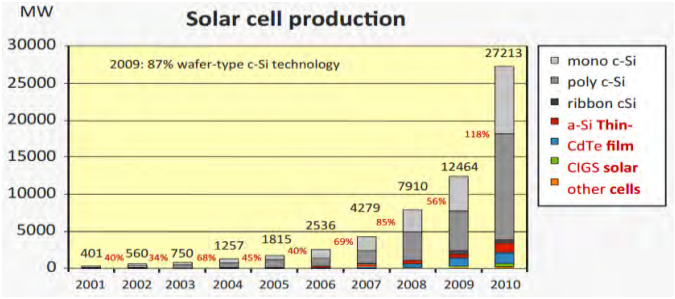

Figure 8.1 Worldwide solar cell production

The solar cell production is increasing exponentially. The percentage numbers represent the annual relative increase in production capacity in reference to the previous year. It shows that the production increases annually by more than 40%, which is an unprecedented growth. Secondly, this graph shows how the various PV technologies contribute to the global module production. The grey colors represent the wafer type c-Si PV technology. As is displayed the c-Si PV technology is the dominant technology and contributes to around 90% of the total module production. The inorganic thin-film PV technologies, like amorphous silicon, cadmium telluride and CIGS, are responsible for the remaining 10%. Figure 8.2 shows the worldwide cumulative installed PV power, which is exponentially increasing in time as well. The different colors reflect the different regions in the world: the green area corresponds to Europe, which shows that the far majority of PV systems are installed in Europe. In conclusion, the Asia Pacific region (shown in light blue) is a good second, where most of the PV power are installed in Japan.

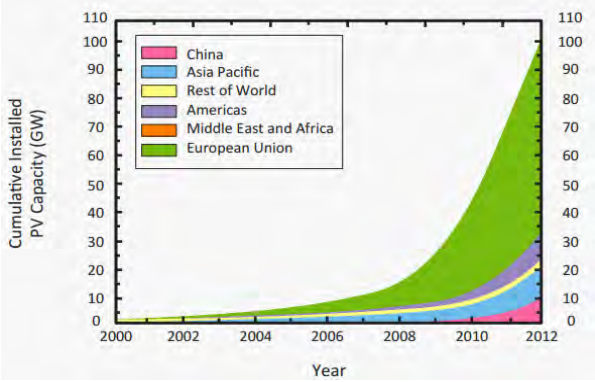

Figure 8.2 Worldwide cumulative installed PV power

The further down corresponds to China, which shows an unprecedented increase in the installed PV capacity from 2010 to 2012. This area reflects the PV capacity installed in North and South America. The third area starting from the bottom corresponds to the rest of the world.It is important to note that the total

installed solar power has passed the 100 GW mark in 2012. The Figure 8.3 illustrates the relative contribution of various nations to the total installed PV power in 2012.

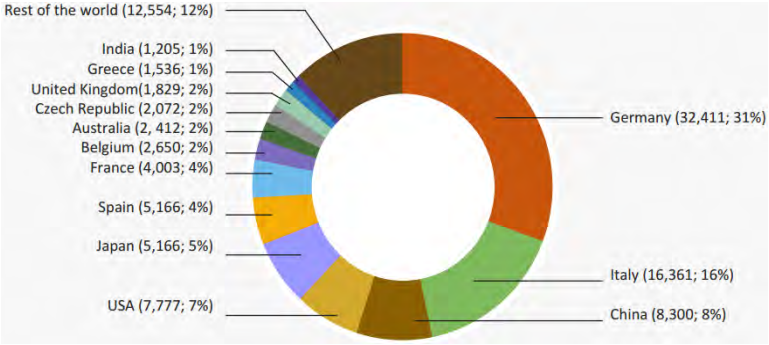

Figure 8.3 Contribution of various nations to the total installed PV in 2012

Here it can be seen clearly that 31% of the total PV capacity is installed in Germany. This is a result of the German government's progressive feed-in tariff policy of the last 10 years. Considering that Germany lies within an area with a relatively low radiation level compared to the rest of the world, the large contribution of solar to Germany's electricity production shows the promising potential of solar energy for the sunnier parts of the world. The runner up is Italy, which accounts for 16% of the worldwide PV capacity. China with a contribution of 8% is the fastest growing market at the moment. In 2010, China only contributed with 2% to the global PV capacity. The United States, Japan and Spain are the other countries in the top 6, with a relative contribution of 7 to 5% to the worldwide installed PV capacity. Note, that after the Fukushima disaster, the Japanese government introduced some progressive feed-in tariffs to promote and speed up the introduction of renewable energy sources.

An interesting aspect of PV technology is that it is not only a European affair. The local demand and supply has been changing rapidly in the last 13 years. Figure 8.4 illustrates the evolution of the worldwide supply and demand of PV modules in the various regions around the world.

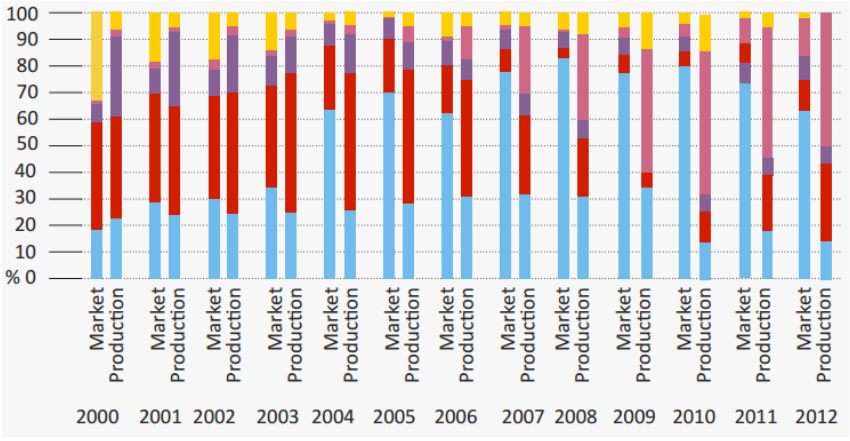

Figure 8.4 Evolution of the worldwide supply and demand of PV modules

Blue represents Europe, red represents the Asia Pacific (mainly Japan), purple the Americas (mainly the United States) and pink represents China. This figure shows that in 2000, the biggest market with a total share of 40% was in Japan. From that moment, due to the introduction of various subsidy policies in Germany, Spain and Italy, the European market share increased up to 80% by the year 2008. Around this

time, the PV market appeared to be a local European affair. From 2009 the domestic PV market in China, the Americas and Asia Pacific are increasing very rapidly as well and catching up quickly with Europe. The Asia Pacific share on the market was increasing. Up to 2006 the European share was increasing slowly. From 2008 we see a big growth of production in China, made possible by huge investments of the Chinese government into scaling up PV module manufacturing in China. In 2012, around 60% of all PV modules were produced in China. In 2000, the PV market was an essential local market mix. The local demand and supply in Asia, Americas and Europe were in balance. By 2012 no local balance between supply and demand exists anymore. The majority of the demand is in Europe whereas the majority of the production is in China.

The PV market has transformed from a local market of demand and supply to a global market of demand and supply. Another aspect that controls demand is the cost price of PV technology. The success of penetrating existing and new PV markets depend on many variables, including:

- costs in $/Wp, as well as $/m2 of product and power availability (kWh/Wp/annum);
- the technical and environmental profile of each newly introduced technology;
- ease of production and the scale at which a production plant becomes economically feasible.

In order to understand how does the cost price of electricity generated by a PV system can be compared to the electricity delivered by energy companies, we can start from the learning curve in Figure 8.5 The learning curve is the graph which shows how the cost price, or in this case the sales price is dropping in time.

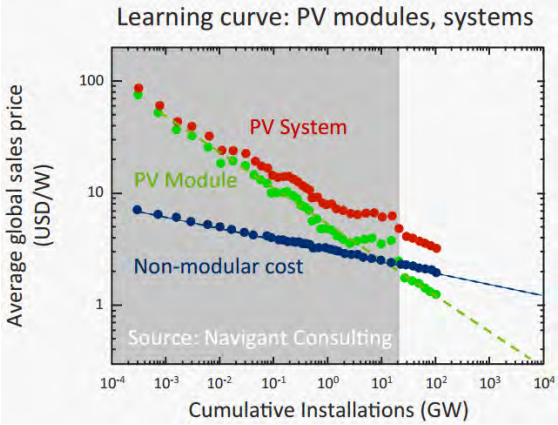

Figure 8.5 Cost of photovoltaic system extrapolation

In time, the industry gets more experienced. Progress in technology provides for better PV modules with higher efficiencies. This experience results in better and faster processing, leading to higher production yields. Up-scaling of production leads to lower cost of source materials. Learning curves usually show an exponentially decreasing cost price in time, until the technology or product is fully developed. In this graph we have the average global sales prices of a PV module versus the cumulative installed power up to 20 GW. Note, that the points up to 20 GW in the grey area are real data points (up to 2009). The points in white area are extrapolations of the general trend. Also important to note is that the sales prices, discounting some fluctuations, follow a largely exponential decay. Currently, the average retail price of only PV module is below 1 dollar per watt-peak. Nevertheless, the cost price of a PV system is not only determined by the module.

The highest curve show the decrease in the cost price of a complete PV system. As is shown, in the early days of the PV technology, the system price was dominated by the module price, however, in the current situation the contribution of the non-modular components starts to play the most dominant role. Non-modular components contain components like the racking, wiring, inverter, battery for stand-alone systems, or even maintenance costs. The difference between the red and green line corresponds to the non-modular costs and is Indicated by the lowest-slope markers.

This shows the learning curve of the non-modular components, which is dropping

not as fast as the module price. This means that nowadays the reduction in the cost price of a PV system will be mainly limited by the cost price of the non-modular components. This shows the advantage of c-Si PV technology, which has higher module efficiencies ranging from 14% up to 20% in reference to thin-film technologies.

Higher conversion efficiency means higher yields per area. While the non-modular cost per area are the same, the cost price per watt-peak of the non-modular cost will be consequently lower for modules with higher conversion efficiencies.

Hydropower is responsible for 19% of the total worldwide electricity production and nuclear is 16%. How do these numbers can be compared to solar? For that, we can use the following graph in logarithmic scale, Figure 8.6.

On the vertical axis you see the cumulative installed capacity which is expressed in GW of power. Here are only considered the energy sources, which are not based on fossil fuels. The installed nuclear power is hardly growing anymore, whereas the installed hydropower is still slightly growing in time. Wind is growing at a relative rate of 20% per year. From 2008 solar is the fastest growing energy technology with a rate far above 40%.

However, it is not fair to compare the installed power between technologies like this. The numbers given here represent the maximum power the energy source can produce, but it is not the average power the electricity source has delivered in reality.

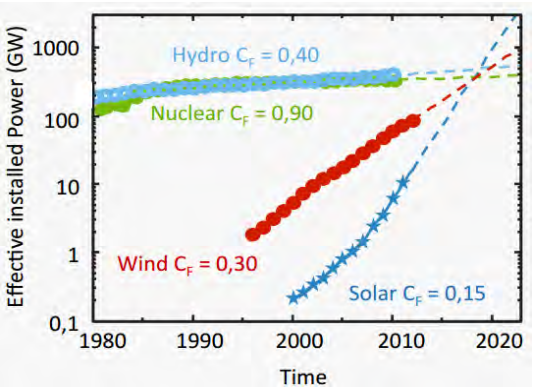

Figure 8.6 Comparison between sources

The relation between these two is called the capacity factor, which is basically a measure of how often an electric generator runs for a specific period of time. Nuclear has with 90% the highest capacity factor, followed by hydropower with an average capacity factor of around 40%. Energy is assumed an averaged capacity factor of 30% for wind and of 15% for solar capacity factor .

A low capacity factor for PV systems can be explained by the fact that for most geographical locations, almost half of the solar day is devoid of solar radiation at
night time. Currently, solar energy generates an order of magnitude less electricity than hydro and nuclear. If we extrapolate the trend of the last decade we see that the installed power of solar energy will exceed nuclear, wind and hydropower by the end of this decade. It is just a matter of time that solar becomes the most important energy source not based on burning fossil fuels.

Solar energy is everywhere and available in great abundance.The total amount of energy in solar light incident on our planet is 10000 times larger than our total energy consumption. By evaporation of water due to solar heat, Hydroelectricity is a secondary form of solar energy.

By solar induced temperature differences, wind is a secondary form of solar energy.

Consequently, solar energy is the biggest renewable energy source around. Hydro, nuclear and wind are centralized electricity generation concepts. It means that it is necessary a big dam, big nuclear plant, or a wind park to generate electricity. Building these large systems requires governmental involvements and big investors.

PV systems can be installed centralized in large solar farms too, however, the unique
advantage here is that PV systems can be installed decentralized as well. Many consumers of electricity can put their own PV system on their home. They become their own producer independent of the market.

Another relevant factor is that in most parts of the world the cost price of a PV system has met or dropped below grid parity. This means that having your own PV system is cheaper than buying the electricity from the grid. The installation of the decentralized PV systems will be the big force behind the solar revolution of the coming years and will change the energy landscape much faster than most people think. As more and more people become aware of this, it is more likely that the growth will be further enhanced than it will be slowed down.

Section 2

1. Comparative study on renewable energy subsiding systems between Italy and Turkey

In this section I will illustrate the situation of the two countries concerning photovoltaic spread and renewable energy sources penetration into the market. In order to understand the role of the government and to have an idea about the time necessary to implement new technologies in the market, the Italian situation will be illustrated first.

1.1. Feed-in scheme(Conto Energia)

The history of photovoltaic technology in Italy starts with the aim to fulfill the requirements of Kyoto Protocol firstly and the 2020 target secondly.

The Official journal of the European Parliament issued the Directive 2001/77/EC on the promotion of electricity from renewable energy sources in the internal electricity market on September 27th 2001. This event can be seen as a result of several suggestions, in particular the resolution of March 30th 2000 which previously underlined the need to establish ambitious targets. Those targets need to be considered also on national level.

The directive highlights the underuse of renewable energy sources in the European community. Therefore, in order to accomplish the achievement of Kyoto targets, it is necessary to increasingly sustain renewable energy sources considering their contribution to environmental protection. Member States had to issue a report every two years about their achievement until 2010. Furthermore, member States had the obligation to guarantee that the origin of the energy produced comes from renewable sources. This operation of verification will be provided by an expert and not be involved in production and distribution of energy that is an independent authority.

Curiosity

The first person who introduced the idea of Feed-in tariff was the former United States president Jim Carter in 1978.Carter during his mandate installed photovoltaic panels on the roof of the White House which subsequently ware removed by later president Ronald Reagan. Now the panels are in the Chinese museum.

1.2. First Feed-in scheme

First Feed-in scheme (D.M. July 28th 2005, reviewed in D.M. February 6th 2006) replaces the previous subsiding system for energy produced by photovoltaic sources. Before the birth of the first feed-in scheme the system supported 50 to 75 % of the total expenses of the photovoltaic plant. On the other

hand, first feed-in scheme adopts subsiding method based on the energy produced by a plant. The surplus of the energy can be sold to the grid for a favored price. In this manner private citizens can connect to the grid and sell energy produced by photovoltaic plants [7].

In this way, subsidies don't lie on government's budget directly, which is a plus for this kind of incentivisation. Furthermore, it is a sign of moving forward to a self-sufficient technology.

The decree had the aim of incentivisation of 100 MW of photovoltaic plants starting from July 28th 2005 . On February 6th 2006 this aim was enlarged to 500 MW with a general score of 1000 MW to be achieved by 2015. It is important to notice that today the total power installed in Italy is 17 714 MW with 550579 plants [8]. Therefore the objective set in 2006 has been successfully achieved.

Subsidies will last for 20 years for all those plants that are ranged between
1 kW to 1000 kW connected to the grid.

Small plants up to 20 kW can choose between net metering scheme or assignation of energy to the grid. On the other hand, plants that exceed the limit of 20 kW of power can benefit from:

- reward from twenty years subsidy based on kW produced and inputted into the grid
- income from sells of surplus to the local grid.

The Decree of February 6th 2006 introduced some interesting changes: in the first place a limit of installed power was set. To be specific, 60 MW for plants up to 50 kW and 25 MW for plants over 50 kW. Secondly, plants with nominal power greater than 50 kW should attach with the incentivisation application a statement of commitment for construction. Moreover the person in charge should deposit an amount of money as guarantee to Supervisor of National Grid for Transmission (GRTN Gestore della Rete di Trasmissione Nazionale). The deposit varies depending on the size of the plant. Thirdly, the application for the plants that use thin-film modules compliant with regulation CEI 61646 (82-12) should be presented only by legal entity. Fourthly, plants that were rejected at first, will have the precedence to be obtain subsidies. This was possible because the incentivized power rose. Therefore first existing plants could start to product and after those new one could became operative.

1.3. Second Feed-in scheme

The decree of Ministry of Economic Development from February 19th 2007 which becomes operational in April 13th 2007 after th adoption of resolution n° 90/07 of Authority of Electric Energy and Gas (AEEG). This new program defines new methods for incentivisation of energy produced by photovoltaic sources.

The main differences with respect to the first feed-in scheme are:

- Abolishment of the preliminary application for the subsidies, in other words first the plant is built and then the application is made
- There are no more annual limits for installation but there is a global limit of 1200 MW of incentivized power
- Tariffs are more brunch out in order to promote small size plants to be integrated in structures and buildings
- Rewards were introduces for smart and efficient use of energy and combination of renewable systems

- The limit for incentivisation of 1000kW for a single plant was removed and restrictions of use of thin film was removed as well, since the thin film technology is suitable to be integrated into the buildings.
- Total amount of incentivized energy was risen to 3000 MW
- Building energy valuation became mandatory just for further reward no longer for access to the subsidies.

The procedure and constriction are quiet the same for both feed-in schemes. Obviously one cannot benefit twice from different feed-in scheme for the same plant. The responsible authority should communicate the acceptance of the application within 60 days after the submission. As I briefly mentioned the Second feed-in scheme has different tariffs. The tariffs for energy produced by photovoltaic plants is defined according to the size of the plant (kW), type of the plant and run date of the plant. Moreover Second feed-in scheme define three types of integration in order to assign the most suitable tariff.

Not incorporated plants: are those which modules are installed on the ground or on all surfaces of the urban buildings.

Partially incorporated plants: are those which modules are positioned on the surfaces of urban buildings.

Incorporated plants: are those which modules are integrated into the elements of urban buildings.

	P (kW)	Not incorporated plant	Partially incorporated plant	Incorporated plants
A	1<P<3	0,40	0,44	0,49
B	3	0,38	0,42	0,46
C	P>20	0,36	0,40	0,44

Table 1.3.1 Value in euro of kWh produced by photovoltaic plant

As it is possible to see in the Table 1.3.1 the highest unitary benefit goes to small domestic incorporated plants. The reason is the promotion of the spread of the photovoltaic generation among the national population. In this manner combining photovoltaic generation with other efficient technologies will be possible, obtaining almost zero energy buildings. The tariffs from the table can be increased by 5 % in the following cases:

- If the photovoltaic plant is greater than 3 kW, architecturally incorporated and responsible subject achieves the title of autoproducer. Auto-producer are those who consume at least 70% of produced energy according to art. 2 Legislative Decree n. 79 of march 16th 1999
- For plants whose the responsible subject is a public school or a public health organization
- Plants incorporated in buildings, structures and buildings used for agricultural purposes as a substitute of fibre cement (Eternit) roofs. In this case the plant may have the same dimensions or smaller with respect to the reclaimed area.
- Plants whose responsible subjects are municipalities with less than 5000 resident according to the last census.

In addition the Second feed-in scheme support rewards for smart and efficient usage of energy. The reward for efficient use of energy is for buildings with plants up to 20 kW provided with net metering collection system. The main requisite is the certificated primary energy reduction of 10 %.

1.4. Third Feed-in scheme

On the 25th of August 2010 the Third feed-in scheme a decree by the Italian Ministry of Economic Development in agreement with the Ministry of Environment, entered into force, setting out the incentives for the production of electricity by photovoltaic (PV)plants.

In relation to the tariffs applicable until 31 December 2010 under the second feed-in tariff, the 2011 tariffs have suffered cuts of between 4.73 per cent and 36.25 per cent, depending on the type and size of the PV plant on the date of its grid connection. Nevertheless, tariff reduction is not the only aspect of the Third feed-in scheme that deserves attention. With the goal of achieving an overall target of 8,000 megawatts (MW) of nominal PV capacity installed on Italian territory by 2020, the Third feed-in scheme makes available funds for 3,000 MW of installed ordinary PV plants. The third feed-in scheme defines the feed-in tariffs applicable to PV plants that started operating between 2011 and 2013. Under a transitional regime introduced by Law no. 129 of 13 August 2010, however, PV plants that started operating by 30 June 2011 may still benefit from the 2010 feed-in tariff provided under the previous tariff scheme on the condition that the end of construction had been communicated to the competent public administration, local grid operator and the (GSE) on or before 31 December 2010.

Unlike the Second feed-in scheme, the Third feed-in scheme no longer distinguishes between ground-mounted, partially integrated and fully integrated PV plants. Instead, it provides two tariff classes:

- PV plants installed on buildings
- Other PV plants

In order to secure a smooth reduction of the feed-in tariff from 2010 to 2011 and to avoid a traumatic impact on projects currently under development or construction, the Third feed-in scheme provides a successive reduction of the tariff in three four-month periods. The Tables below show the tariff system for ordinary PV plants in 2011.

Power class	1 January 2011 to 30 April 2011		
	PV plants installed on buildings	Arbours, greenhouses, sheds, acoustic barriers	Other type of PV plant
KW	€/KWh	€/KWh	€/KWh
1≤P≤3	0.402 (-4.73%)	0.382 (-18.72%)	0.362 (-5.73%)
3<P≤20	0.377 (-6.45%)	0.358 (-19.00%)	0.339 (-7.12%)
20<P≤200	0.358 (-6.77%)	0.3395 (-19.54%)	0.321 (-7.22%)
200<P≤1000	0.355 (-7.55%)	0.3345 (-20.73%)	0.314 (-9.24%)
1000<P≤5000	0.351 (-8.59%)	0.332 (-21.32%)	0.313 (-9.53%)
P>5000	0.333 (-13.28%)	0.315 (-25.35%)	0.297 (-14.16%)

Table 1.4.1 Incentives between January 1st 2011 and April 30th 2011

Power class	1 May 2011 to 31 August 2011		
	PV plants installed on buildings	Arbours, greenhouses, sheds, acoustic barriers	Other type of PV plant
KW	€/KWh	€/KWh	€/KWh
1≤P≤3	0.391 (-7.34%)	0.369 (-21.48%)	0.347 (-9.63%)
3<P≤20	0.360 (-10.66%)	0.341 (-22.85%)	0.322 (-11.78%)
20<P≤200	0.341 (-11.19%)	0.325 (-22.98%)	0.309 (-10.69%)
200<P≤1000	0.335 (-12.76%)	0.319 (-24.40%)	0.303 (-12.42%)
1000<P≤5000	0.327 (-14.84%)	0.308 (-27.01%)	0.289 (-16.47%)
P>5000	0.311 (-19.01%)	0.293 (-30.56%)	0.275 (-20.52%)

Table 1.4.2 Incentives between May 1st and August 31 2011st

Power class	1 September 2011 to 31 December 2011		
	PV plants installed on buildings	Arbours, greenhouses, sheds, acoustic barriers	Other type of PV plant
KW	€/KWh	€/KWh	€/KWh
1≤P≤3	0.380 (-9.95%)	0.3565 (-24.14%)	0.333 (-13.28%)
3<P≤20	0.342 (-15.13%)	0.323 (-26.92%)	0.304 (-16.71%)
20<P≤200	0.323 (-15.88%)	0.304 (-27.96%)	0.285 (-17.63%)
200<P≤1000	0.314 (-18.22%)	0.290 (-31.27%)	0.266 (-23.12%)
1000<P≤5000	0.302 (-21.35%)	0.283 (-32.93%)	0.264 (-23.69%)
P>5000	0.287 (-25.26%)	0.269 (-36.25%)	0.251 (-27.45%)

Table 1.4.3 Incentives between September 1st and December 31 2011st

The percentages in parenthesis show the tariff reductions in relation to the 2010 tariffs. "PV plants installed on buildings" are compared to "partially integrated PV plants" under the Second feed-in scheme 2010, while "greenhouses, sheds, acoustic barriers" are compared to the "fully integrated PV plants". It is important to note that the percentage reduction in tariff is not equal to the percentage of reduction in proceeds generated by a PV plant, given that the proceeds of a PV plant are composed of the sum of the feed-in tariff and the sale price of the electricity.

PV plants that only started operating in 2012 or 2013 are entitled to the feed-in tariff applicable to the last four-month period of 2011, reduced by 6 per cent per year.

1.4.1. Awards

The Third feed-in provides certain premiums for specific types, location and applications of PV plants. In particular:

- Ground-mounted PV plants (*i.e.,* those neither installed on buildings nor in greenhouses, sheds or acoustic barriers), which are located in areas qualified by the applicable zoning plan as industrial or commercial areas, rubbish dumps or contaminated areas, are entitled to a 5 per cent increase in base tariff.
- PV plants constructed by municipalities with less than 5,000 inhabitants are entitled to a 5 per cent increase in base tariff if they are installed on buildings and operate under the net-metering regime.
- PV plants that are installed on buildings benefit from a 10 per cent increase in base tariff in the event that they replace roofs containing asbestos.

Only one of the above premiums can apply to each PV plant. They cannot be used in combination with each other. Other premiums apply to PV plants that are combined with efficient use of energy or a system of predictable electricity input.

1.4.2 Integrated PV Plants with Innovative Features

Integrated PV plants with innovative features describe PV plants composed of innovative modules and components specifically developed to integrate and substitute architectural elements of buildings. 300 MW of these plants will be subsidised by a specific tariff. Integrated PV plants with innovative features that start operating between January 1st 2011 and December 31st 2011 will benefit from the feed-in tariffs.

Power range	Feed-in tariff
KW	€/KWh
1≤P≤20	0.44 (-0.45%)
20<P≤200	0.40 (-5.21%)
P>200	0.37 (-12.32%)

Table 1.4.2.1 Feed-in tariff for innovative features

The reduction shown in the table is in relation to fully integrated plants of Second feed-in scheme.

1.4.3. Concentrated Photovoltaic Plants (CPV)

Concentrated photovoltaic (CPV) plants must not be confused with CSP (concentrated solar power) systems. CPV are PV plants where optical systems allow the concentration of sunlight on the photovoltaic cells. 200 MW of CPV plants will be subsidised by a specific tariff.

The feed-in tariff of the Third feed-in scheme applies to CPV plants with immediate effect, not just from January 1st 2011. CPV plants that started operating before December 31st 2011 will benefit from the feed-in tariffs listed below.

Power range	Feed-in tariff
KW	€/KWh
1≤P≤200	0.37
200<P≤1000	0.32
P>1000	0.28

Table 1.4.3.1 CPV tariffs

The reduction of the feed-in tariff for CPV plants that started operating after 31 December 2011 will be 2 per cent per year[9].

1.5. Fourth feed-in tariff scheme

The Fourth feed-in scheme replaces the Third feed-in scheme incentive system intended to provide the support system for photovoltaic (PV) plants between 2011 and 2013.

PV installations in Italy had grown exponentially being supported by three precedent feed-in schemes which are the result of an extra charge on the citizen's electricity bill. Indeed this extra charge became unsustainable, the Government enacted in March 2011 the Legislative Decree no 28/2011 (the so-called Renewables Decree), which imposed on the Ministry of Economic Development the immediate revision of the incentive system.

As the precedents also did the Fourth feed-in scheme provides a differentiated incentive system, depending on the type and size of the PV system. The major changes consisted in a significant reduction of incentives with respect to the Third feed-in tariff. Specific expense budgets have been established for large PV plants for three intervals between June 2011 and December 2012. These budgets shall be enforced through a complex ranking system with the aim to limit the access of large PV plants to the incentives. Moreover it will be applicable to large PV plants that became operative after September 1st 2011.

Starting in 2013, pre-established half-yearly expense budgets had to be respected through additional tariff reductions applying to all PV plants based on previous installations. No incentives had to be awarded to PV plants entering into operations after 2016, as the Government apparently expects full grid parity to be reached in 2017.

In Fourth as in the previous feed-in schemes, until 2012 incentives will be paid as a feed-in premium that comes in addition to the price for the sale of electricity. Feed-in premiums are differentiated depending on the type of PV plant:

- PV plants integrated in buildings and using innovative technologies
- PV plants using concentration technology
- "Ordinary" PV plants, i.e. all other PV plants that do not fall under the first two categories

Within these categories the premiums decrease according to the size of PV plant and starting date.

With regard to ordinary PV plants, Feed-in premiums will decreased on a monthly basis in 2011, whereas reductions operated half-yearly in 2012. Relevant for the applicable premium period is the start of operations of the PV plant.

In this respect, the Fourth Feed-in scheme provides that, in cases where late start of operations depends on the grid operator and not on the applicant, and this circumstance implies the loss of a specific tariff, the applicant shall receive the reimbursement provided by the Authority for Energy and Gas (Resolution no. 181/10)[2].

Power Class	June 2011		July 2011		August 2011	
	PV Plants Installed on Buildings	Other PV Plants	PV Plants Installed on Buildings	Other PV Plants	PV Plants Installed on Buildings	Other PV Plants
1≤P≤3	0.387 (-1.02%)	0.344 (-0.86%)	0.379 (-3.06%)	0.377 (-2.88%)	0.368 (-5.88%)	0.327 (-5.76%)
3<P≤20	0.356 (-1.1%)	0.319 (-0.93%)	0.349 (-3.06%)	0.312 (-3.11%)	0.339 (-5.83%)	0.303 (-5.90%)
20<P≤200	0.338 (-0.88%)	0.306 (-0.97%)	0.331 (-2.93%)	0.300 (-2.91%)	0.321 (-5.87%)	0.291 (-5.83%)
200<P≤1000	0.325 (-2.99%)	0.291 (-3.96%)	0.315 (-5.97%)	0.276 (-8.91%)	0.303 (-9.55%)	0.263 (-13.20%)
1000<P≤5000	0.314 (-3.98%)	0.277 (-4.15%)	0.298 (-8.87%)	0.264 (-8.65%)	0.280 (-14.37%)	0.250 (-13.49%)
P>5000	0.299 (-3.86%)	0.264 (-4%)	0.284 (-8.68%)	0.251 (-8.73%)	0.269 (-13.5%)	0.238 (-13.45%)

Table 1.5.1 Incentives monthly reduction

Power Class	1st Semester 2012		2nd Semester 2012	
	PV Plants Installed on Buildings	Other PV Plants	PV Plants Installed on Buildings	Other PV Plants
1≤P≤3	0.274 (-23.25%)	0.240 (-23.33%)	0.252 (-29.41%)	0.221 (-29.39%)
3<P≤20	0.247 (-23.05%)	0.219 (-23.43%)	0.227 (-29.28%)	0.202 (-29.37%)
20<P≤200	0.233 (-23.36%)	0.206 (-23.13%)	0.214 (-29.61%)	0.189 (-29.48%)
200<P≤1000	0.224 (-24.07%)	0.172 (-31.2%)	0.202 (-31.53%)	0.155 (-38%)
1000<P≤5000	0.182 (-35.92%)	0.156 (-37.10%)	0.164 (-42.25%)	0.140 (-45.55%)
P>5000	0.171 (-36.64%)	0.148 (-37.29%)	0.154 (-42.94%)	0.133 (-45.64%)

Table 1.5.2 Incentives half-yearly reduction

The numbers in the tables indicate the percentage of premium reduction in respect of the feed-in premiums that had originally been provided by the Third Feed-in scheme for the same period.

The feed-in premiums indicated in the table are further increased by the following increments:

- 5 per cent for ground-mounted PV plants located in industrial or commercial areas, waste treatment areas, exhausted quarries or polluted areas
- 5 per cent for small PV plants managed by municipalities with fewer than 5,000 inhabitants
- 5 Eurocents per kW/h for rooftop PV plants replacing asbestos
- 10 per cent to PV plants whose cost of construction, excluding work costs, is composed at 60% or more by components manufactured within the European Union

Higher feed-in premiums are granted to integrated PV plants using innovative technologies. These PV plants should be built on rooftops using innovative modules and components specifically developed to substitute architectural elements of buildings. Integrated PV plants with innovative features that started operating between June 1st 2011 and December 31st 2011 and between January 1st 2012 and December 31st 2012 will benefit from the feed-in tariffs listed in theTable 1.5.3.

Power Range	June – December 2011	1st Semester 2012	2nd Semester 2012
kW	EUR/kWh	EUR/kWh	EUR/kWh
1≤P≤20	0.427 (-2.96%)	0.418 (-3.06%)	0.410 (-4.92%)
20<P≤200	0.388 (-3%)	0.380 (-3.06%)	0.373 (-4.85%)
P>200	0.359 (-2.97%)	0.352 (-2.92%)	0.345 (-4.85%)

Table 1.5.4 Incentives for integrated plants

The numbers in the table indicate the percentage of premium reduction in respect of the feed-in premiums that had originally been provided by the Third Feed-in scheme for the same period.
As it has been mentioned before, also concentrated photovoltaic plants are considered in the Fourth Feed-in scheme. Those plants that meet technical requirements can benefit tariffs listed in Table 1.5.5.

Power Range	June – December 2011	1st Semester 2012	2nd Semester 2012
kW	EUR/kWh	EUR/kWh	EUR/kWh
1≤P≤200	0.359 (-2.97%)	0.352 (-2.92%)	0.345 (-4.85%)
200<P≤1000	0.310 (-3.12%)	0.304 (-3.06%)	0.298 (-4.97%)
P>1000	0.272 (-2.86%)	0.266 (-5%)	0.261 (-4.88%)

Table 1.5.5 Incentives For concentration plants

The numbers in the table indicate the percentage of premium reduction with respect to the feed-in premiums that had originally been provided by the Third Feed-in scheme for the same period.

1.5.1. Ranking system and restrictions for large PV plants

The ranking system that is explained below entered into force for plants which started operating after 31st of August 2011. Moreover the owners had to communicate to the GSE the date of entrance in operation 15 days before the effective entrance into operation.
The owners of large PV plants that started operations after 31st of August 2011 had to file all the applications with GSE between May20st and June 30st. If the available budget for 2011 was not reached after the closing of the registration period on 30 June 2011, the GSE was to open a further application period between 15 and 30 September 2011. Furthermore if the cumulated expenses related to PV plants approved to the incentives exceeded the available budget for 2011, the 2012 budget had to be be reduced according to 2011 extra costs.
For the first semester of 2012, the applications had to be filed with the GSE from 1 to 30 November 2011. In case the budget was not reached GSE was to open further application period until the available budget

is reached. Within 15 days from the end of registration period GSE publishes a ranking list based on importance criteria:

- PV plants that are operational at the date of filing of the application to the GSE
- PV plants for which the construction works have been completed at the date of filing of the application with the GSE (in such case, the applicant shall file the certificate of completion of the works within the closing of the registration period)
- Date of the building permit (oldest permits have priority)
- Minor nominal power of the PV plants
- Date of application for registration in the ranking list (oldest have priority)

With regard to work completion and late completion penalty it is necessary to know following details.
The feed-in premium shall be granted to large PV plants only at the condition that construction works are completed. Specific completion certificate should be delivered to the GSE, within seven months or nine months in case of plants exceeding 1 MW as of the date of publication of the ranking list.
If construction works are not completed within the mandatory time period, the registration from the ranking list will be annulled. The PV plant may then still be admitted to the feed-in premium of a subsequent period, but the respectively applicable feed-in premium will be reduced by a penalty of 20 per cent.

1.6. Fifth feed in scheme

The Ministerial Decree of July 5th 2012 published on July 10th 2012 is the so called 5th feed-in scheme which redefines the rules about support for solar photovoltaic power generation.
This new Decree was enacted on August 27th 2012 after AEEG's (Autorità per l'energia elettrica e il gas) Decision (292/2012/r/efr of 12 July. 2012) which is based on GSE's data and it underlines that indicative yearly cumulative cost of incentives has reached Euro 6 billion.
The Fifth feed-in scheme will cease to have effect 30 calendar days after reaching an indicative cumulative cost of incentives of Euro 6.7 billion per year (including costs allocated for plants whose position in the relevant Registries does not exceed the applicable cost limit)[10]. Based on the data reported by GSE through its Photovoltaic counter, AEEG will determine the cessation of the scheme.
The Fourth feed-in scheme will remain in charge for the following types of plants:

- PV plants constructed on land or buildings owned by Public Administration (PA)as long as they start operating on or before 31 December 2012
- Large PV plants that have obtained a registration in 2012 raking list and provide that the construction works are completed within 7 months for plants which don't exceed 1 MW and nine months for plants over 1 MW.
- Small PV plants, concentrating PV plants and PV plants with innovative features if they commence operations before 27 August 2012

All those PV plants that have not obtained a registration in the GSE 2012 ranking list and are not installed on property of PA cannot be candidate for Fourth feed-in scheme even if their starting date is before August 27th 2012. , Therefore they will be subject of Fifth feed-in scheme.

1.6.1 Access to incentives

There are mainly two ways for the access to incentives depending on the plant's size and type. The first way is to send a simple application without any budget restriction and the second is through registration and ranking system aimed at distributing fairly the available budget.
For direct access to the incentives only the following plants can benefit without any budget restriction:

- PV plants not exceeding 50 kWp, built on rooftops and replacing asbestos.
- PV plants not exceeding 12 kWp, including refurbished PV plants and PV plant refurbishments not exceeding 12 kWp.
- Integrated PV plants that use innovative technology, but only until the aggregate annual cost of incentives for this type of PV plant has reached €50 million.
- Concentrating PV plants, but only until the aggregate annual cost of incentives for this type of PV plant has reached €50 million.
- PV plants managed by public administrations after a public tender procedure has been carried out, but only until the aggregate annual cost of incentives for this type of PV plant has reached €50 million.
- PV plants having nominal power of between 12 kWp and 20 kW, including refurbished PV plants.
- PV plant refurbishments not exceeding 20 kWp, that apply for a FiT reduced by 20 per cent of the regular feed in tariff applicable to PV plants of the same size.

1.6.2. Access through the GSE ranking system

All those plants that do not meet the requirements for direct access to the feed-in tariff must apply to the GSE for access in a special register. In order to obtain the feed-in tariff they must achieve a sufficiently high position to be included in one of the following registers:

- First register: €140 million
- Second register: €120 million
- Subsequent registers: €80 million, up to the €6.7 billion threshold.

It is possible to see that starting from the second register the budget will be reduced progressively until the achievement of 6.7 billion.
The ranking criteria gives the highest priority to the starting date of the operation. The operation starting date is in first place in order to protect projects that were developed under the Fourth feed-in scheme and

that should start operating when the Fifth feed-in scheme entered in force. After this first criterion which is reserved just for first register there is a list for the rankings in order of priority.

The feed-in tariff is granted for a period of 20 years starting from the date the PV plant commenced operating, or in cases of delayed application, on the date the application is received

With respect to the amount of feed-in tariffs ordinary plants are entitled to payments depending on whether they feed the produced electricity in the grid or the electricity is self-consumed Tables 1.6.2.1 and 1.6.2.2.

The feed-in tariff listed in Table 1.6.2.1 for PV plants up to 1 MW is intended as an "overall tariff", it includes both a production premium and the price for the sale of the energy produced by the PV plant. It is paid on the net electricity fed into the grid. PV plants with a nominal power exceeding 1 MW are no longer entitled to sell the electricity to the GSE, but have to sell it to the market through bilateral power purchase agreements or through the Power Exchange. Accordingly, the FiT in these circumstances is determined as the difference between the amounts indicated in Table 1.6.2.1 and the applicable average market price (prezzo zonale orario).

	PV Plants Installed on Buildings					Other PV Plants				
	Semester					Semester				
Power Class	I	II	III	IV	V	I	II	III	IV	V
[kW]	[€/MWh]					[€/MWh]				
1≤P≤3	208	182	157	144	133	201	176	152	140	130
3<P≤20	196	171	149	137	128	189	165	144	133	124
20<P≤200	175	157	141	131	122	168	151	136	126	118
200<P≤1000	142	130	118	111	106	135	124	113	107	102
For PV plants with a nominal power exceeding 1000 kWp, the GSE does not purchase the electricity produced but pays a feed-in premium that is determined as the difference between the hypothetical, all-inclusive tariff below and the applicable average electricity market price (*prezzo zonale orario*).										
1000<P≤5000	126	118	110	105	100	120	113	106	101	97
P>5000	119	112	104	99	95	113	106	99	95	92

Table 1.6.2.1 Feed-in tariffs for PV plants

	PV Plants Installed on Buildings					Other PV Plants				
	Semester					Semester				
Power Class	I	II	III	IV	V	I	II	III	IV	V
[kW]	[€/MWh]					[€/MWh]				
1≤P≤3	126	100	75	62	51	119	94	70	58	48
3<P≤20	114	89	67	55	46	107	83	62	51	42
20<P≤200	93	75	59	49	40	86	69	54	44	36
200<P≤1000	60	48	36	29	24	53	42	31	25	20
1000<P≤5000	44	36	28	23	18	38	31	24	19	15
P>5000	37	30	22	17	13	31	24	17	13	10

Table 1.6.2.2 Premiums for self-consumption

	All-Inclusive Tariff					Self-Consumption Tariff				
	Semester					Semester				
Power class	I	II	III	IV	V	I	II	III	IV	V
[kW]	[€/MWh]					[€/MWh]				
1≤P≤20	288	242	218	196	176	186	160	144	130	117
20<P≤200	276	231	208	187	169	174	149	134	121	109
P>200	255	217	195	176	158	153	135	121	109	98
For PV plants with a nominal power exceeding 1000 kWp, the GSE does not purchase the electricity produced but pays a feed-in premium that is determined as the difference between the all-inclusive tariff above and the applicable average electricity market price (*prezzo zonale orario*).										

Table 1.6.2.3 Feed-in tariffs for PV plants using innovative technology

	All-Inclusive Tariff					Self-Consumption Tariff				
	Semester					Semester				
Power class	I	II	III	IV	V	I	II	III	IV	V
[kW]	[€/MWh]					[€/MWh]				
1≤P≤20	259	215	194	174	157	157	133	120	108	97
20<P≤200	238	201	181	163	146	136	119	107	96	87
P>200	205	174	157	141	127	103	92	83	75	67
For PV plants with a nominal power exceeding 1000 kWp, the GSE does not purchase the electricity produced but pays a feed-in premium that is determined as the difference between the all-inclusive tariff above and the applicable average electricity market price (*prezzo zonale orario*).										

Table 1.6.2.4 Feed-in tariffs for concentrating PV plants

1.7. Results of the Italian system

Up to now we have considered the Italian evolution of its incentivisation system. It is important to notice how the system changed over the years in terms of amount of incentivisation and distinction in classes. Nowadays we are experiencing the end of incentives concession it is therefore possible to comment the results. In the next charts some of the most important figures will be shown in order to take a closer look on feed-in schemes achievements.

In the Table 1.7.1 is represented the total amount of the installed power updated as of July 31st 2014. Moreover the table shows how the total amount of power is distributed in all the country taking in account the class of the plants with respect to their power. It is possible to see that achievement was 17,731 GW with Puglia at the first place with 2,5 GW.

	CLASSE 1: 1 kW ≤ P ≤ 3 kW		CLASSE 2: 3 kW < P ≤ 20 kW		CLASSE 3: 20 kW < P ≤ 200 kW		CLASSE 4: 200 kW < P ≤ 1000 kW		CLASSE 5: 1000 kW < P ≤ 5000 kW		CLASSE 6: P > 5000 kW		TOTALE	
REGIONE	Numero	Potenza (kW)	Numero	Potenza (kW)	Numero	Potenza (kW)	Numero	Potenza (kW)	Numero	Potenza (kW)	Numero	Potenza (kW)	Numero	Potenza (kW)
PUGLIA	11.312	31.764	22.164	168.624	2.868	208.666	1.819	1.566.145	56	173.623	36	355.753	38.255	2.504.575
LOMBARDIA	27.422	76.153	38.158	300.781	8.896	710.405	1.340	731.709	61	112.698	3	17.992	76.880	1.949.737
EMILIA ROMAGNA	19.269	50.908	25.772	209.076	5.969	475.103	1.136	708.703	155	284.068	4	48.656	52.305	1.776.513
VENETO	21.572	60.143	45.763	320.693	5.924	475.727	920	523.621	47	80.011	14	160.505	74.240	1.620.700
PIEMONTE	12.311	34.348	20.505	177.538	4.554	365.353	1.089	637.898	93	203.054	4	25.730	38.556	1.443.921
SICILIA	10.915	30.983	24.004	182.221	2.236	172.172	546	396.803	86	243.540	22	186.650	37.809	1.212.369
LAZIO	11.166	30.177	18.665	134.371	1.623	130.623	416	265.091	100	274.650	35	309.040	32.005	1.143.953
MARCHE	5.699	16.383	9.758	80.844	2.384	193.566	936	592.555	50	110.803	3	20.890	19.830	1.017.042
SARDEGNA	8.634	24.474	16.767	117.890	971	77.316	247	152.838	88	185.685	18	138.218	26.725	696.422
TOSCANA	10.611	28.907	14.864	121.185	2.575	204.051	415	248.656	33	59.263	4	33.585	28.502	695.646
ABRUZZO	3.214	9.082	9.248	74.916	1.242	102.191	479	343.080	55	120.341	2	11.851	14.240	661.461
CAMPANIA	5.245	14.923	13.595	101.617	1.315	106.448	340	210.917	49	123.971	11	99.601	20.555	657.476
FRIULI VENEZIA GIULIA	6.383	17.943	15.860	113.015	1.777	137.186	168	100.295	25	69.006	4	27.358	24.217	464.805
CALABRIA	4.549	13.021	11.910	94.994	1.060	77.274	218	129.384	26	53.166	8	80.051	17.771	447.890
UMBRIA	4.603	12.780	6.808	55.171	1.454	104.356	344	226.900	20	43.203	-	-	13.229	442.409
TRENTINO ALTO ADIGE	7.737	21.983	9.039	92.774	2.426	170.734	295	92.127	3	4.931	-	-	19.410	382.549
BASILICATA	1.721	4.921	3.647	33.991	851	50.796	354	248.160	4	8.034	1	5.216	6.578	351.119
MOLISE	585	1.663	2.098	17.742	272	20.054	100	76.722	13	40.618	1	6.500	3.069	163.298
LIGURIA	2.118	5.627	2.487	18.857	301	23.842	53	28.417	3	4.167	-	-	4.962	80.910
VALLE D'AOSTA	538	1.491	1.014	8.786	93	7.228	2	1.440	-	-	-	-	1.647	18.946
Totale ITALIA	176.604	489.675	313.126	2.425.087	48.791	3.813.090	11.127	7.281.461	967	2.194.831	176	1.527.596	550.785	17.731.740

Table 1.7.1 Total results of feed-in schemes updated 31 of July 2014 [11]

In Figure 1.7.2 is shown the trend of the amount of incentives and production starting from 2006. It is possible to see how the growth rate changed in 2011 when Second feed-in scheme entered in charge.

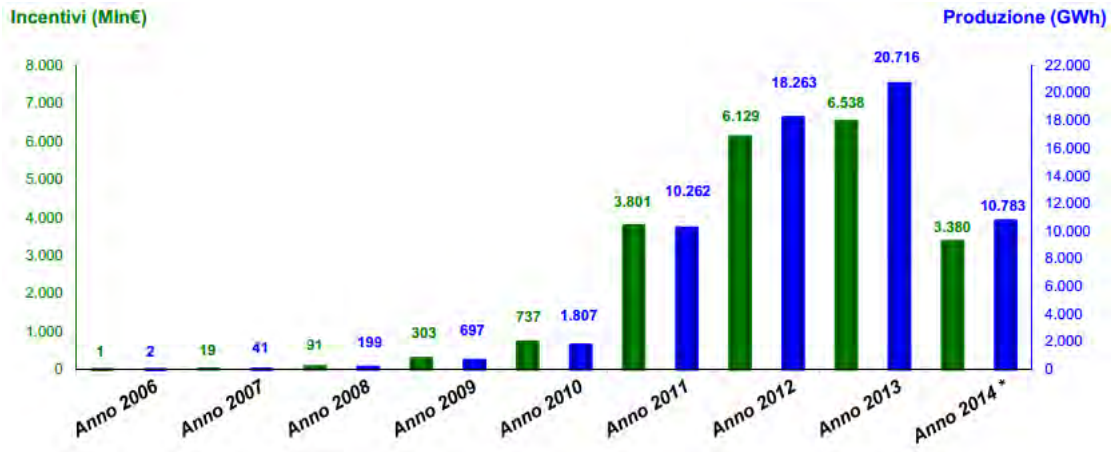

Figure 1.7.2 Investments and production
with regard to Feed-in Schemes

In Figure 1.7.3 is shown the evolution of the installed power in Italy highlighting the respective feed-in scheme supplies.

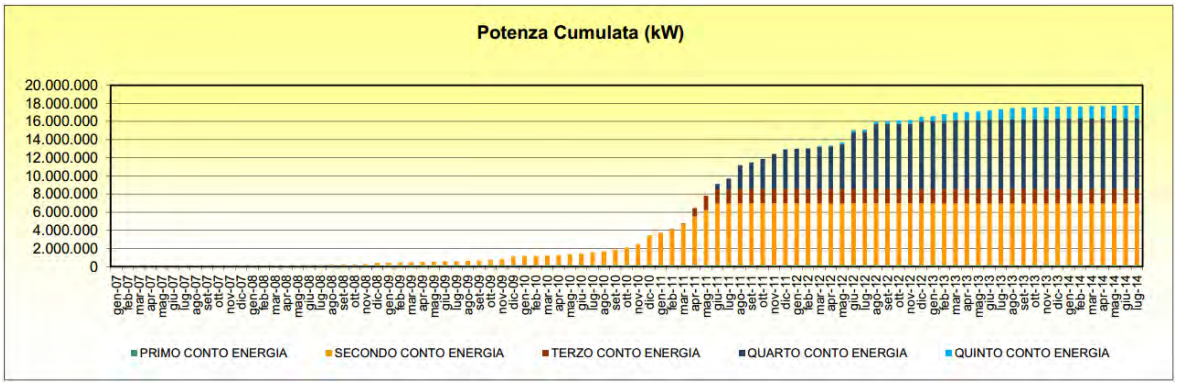

Figure 1.7.3 Power and feed-in schemes [12]

1.8. Turkey subsidies system

Turkey is the 17th largest economy of the World (IEA Turkey, 2009). Turkey's economy has been developing strongly in the last decade. The fast industrialization, growing demand of energy and urbanization require more energy production. The demand for electric energy in Turkey expected to be 580 billion kWh by the year 2020 [13]. Even though Turkey has a rich renewable resources like solar, wind, geothermal, biomass, and hydrogen energy, there is not enough access to such form of energy.

Turkey's primary energy demand is obtained mainly from coal (% 31), gas (% 32), fuel (% 27), and others(% 10-including renewables biomass, wind, hydro geothermal and solar) [3]. On the other hand, Turkey is rich in renewable energy sources due to its geographical location and the geological structure. Beginning from 2008, as a result of the incentives for renewable energy, especially hydraulic, wind, solar and geothermal energy increased its share in the total installed capacity. By the end of 2013, Turkey's installed electricity capacity included 39,6% of renewable energy with 25 596MW, 60% from thermal sources and 0,4 from others. Nowadays Turkey's aim is to increase the electric generation with more participation of renewable energy. The main goals are especially to reach 20 000 MW in wind power installation and to evaluate the potential of solar energy generation. In the recent times the usage of renewable resources in Turkey constitutes 1% of total energy production[14]. In Figure 1.8.1 are shown installed renewable power and estimate renewable power according to Environmental Information Exchange (EIE)[8]

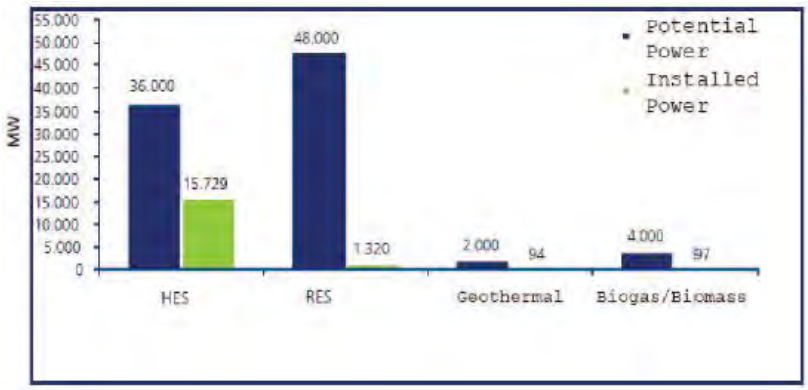

Figure 1.8.1 Renewable energy in Turkey

The first incentivisation for electricity generation from renewable energy sources started with the law No. 4628 in March 2001. According to this law private subjects and corporate entities are exempted from licensing obligations and setting up a company as long as the power plant counts less than 500 kW. The authority which was set up for management of renewable energy license and incentives concession is Energy Market Regulatory Authority (EMRA).

Law No. 5346 on Utilization of Renewable Energy Resources for the Purpose of Generating Electricity" came into force in 2005, aiming to enhance and support the use of renewable energy sources in Turkey in line with free market principles and conditions.

Incentives mechanism introduced by first two laws was mainly:

- Licensing : 1) individual and corporate entities built a electricity generation facilities from renewable energy sources having maximum installed capacity of 500kW(later was set at 1MW) are exempt from licensing and setting up a company

  2) Only 1% of the licensing cost is paid by corporate entities applying to get a license and secondly start to pay annual licensing cost after eight years from operating start
- Land appropriation: 85% discount is applied to rent, right of exemption and usage permits and Forest Villagers Development Revenue, Forestation and Erosion Control Revenues are not demanded during the first 10 years
- Purchase guarantee by a constant feed-in tariff: 1) government guarantees to buy electricity for 10 years from renewable energy plants built or to be build between 18.05.2005 and 31.12.2015. Feed-in tariff changes from plant to plant, in particular: 5,3 €c/kWh for hydropower and wind, 7,65 €c/kWh for geothermal, 9,69 €c/kWh for solar and biomass plants.

  2) Domestic manufacturing of the equipment to be used in power plants is promoted with additional feed-in tariffs ranged between 0,3 and 2,55 €c/kWh depending on the type of renewable energy and equipment.
- The Turkish Electricity Transmission Company (TEIAS) and/or distribution companies are required to give priority status for systems connection of generating facilities based on renewable.

Even though these mechanism were introduced and revised they were still considered inadequate when compared to the EU countries which were leading the utilization of renewable energy sources.

Energy Efficiency Law No 5627 was enacted on the 2nd of May 2007. "The Energy Efficiency Law (EE Law) aims to increase the efficient use of energy and energy resources for reducing the load of energy costs on the economy and protecting the environment. This law comprises the organization, principals and procedures for increasing energy efficiency in industry, electrical power plants, transmission and distribution systems, building service and transport sectors.

It sets the rules for energy management in industry and in big buildings, project supports, energy efficiency consultancy companies, voluntary agreements and so on." Energy efficiency measures in industry are based on the 2007 Energy Efficiency Law and two related by-laws published in October 2008: the By-law on Improving Energy Efficiency for the Utilization of Energy Resources and Energy, and the By-law on Supporting Energy Efficiency of Small and Medium-sized Enterprises (SMEs) including Training, Audit and Consultancy Services. Energy efficiency measures in manufacturing industry focus on energy management, financial support, voluntary agreements, monitoring, and training and awareness.

In power generation, the measures focus on managing demand; improving efficiency of power plants (moreover by setting minimum efficiency requirements for new plants), transmission, distribution and public lighting; utilizing waste heat of thermal power plants; and utilizing alternative fuels.

The law numbered 6094 which came into force on January 8, 2011 developed incentives for the use of renewable energy resources. The Renewable Energy Law aims to encourage energy production from renewable energies by providing incentives. These incentives comprise of energy generation from sources such as wind, solar power, biomass, hydropower and geothermal. The legislative framework adjusts the prices for the sale of electricity to the state according to generation method. According to the law

renewable energy plants will be subjected to prices from 7.3 USD cents to 13.3 USD cents per kWh. A hydroelectric power plant will be able to sell electricity at a cost of 7.3 USD cents (5.6 Euro cents) the same as the amount for a wind farm. The geothermal energy suppliers can sell their electric energy at a price of 10.5 USD cents (8.1 Euro cents). Companies that use biomass (including landfill gas) and solar power are subsidized the most at a rate of 13.3 USD cents (10 Euro cents) per kilowatt-hour. The law also features additional support for companies with facilitates that use locally produced equipments and components Figure 1.8.2.

C- Facilities of photovoltaic solar panels	1.Integration of PV panels and manufacture of the structural mechanics of the solar PV panels	0.8
	2.PV modules	1.3
	3. Cells that make up PV modules	3.5
	4.Inverter	0.6
	5 Beam materials that focusing solar energy on the solar PV module	0.5

Figure 1.8.2 Additional subsidies for usage of local components [15]

The Strategic plan 2015-2019 was the is the result of Ministry's institutional and executive call for policy development to meet the daily requirements of the energy sector and natural sources. Strategic Plan 2015-2019 of the Ministry consists of 8 themes, 16 goals and 62 objectives in total, and involves the following outline: In the field of Energy and Natural Resources, good governance and stakeholder interaction, regional and international effectiveness, technology, R&D and innovation, improvement of investment environment. The common development requirements in the field of energy are to supply security, energy efficiency and saving while in the field of natural resources are efficient and effective raw material use and raw material supply security.. Sustainability is considered as an inevitable concept for the process of introducing energy and natural resources into economy. Their consumption has not been designed as a separate theme but designed as a frame to include all themes. The Strategic Plan has been aimed to be implemented under the consideration of environmental, economic and sustainability principles in terms of its all goals, objectives and strategies.

1.9. Results of Turkish subsiding system

Turkey has a target for more clean and dependable energy production by using renewable energy resources. By signing the Kyoto Protocol Turkey demonstrated its will to give more importance to green energy for its and entire World's future. In 2009, Turkey has announced the Electricity Market and Supply Security Strategy Paper, which aims to rise the share of electricity generated by renewable energy resources amount to a minimum of 30% of total electricity generation. Looking at the current Turkey needs more investments and more laws, which will protect and encouraging investors.

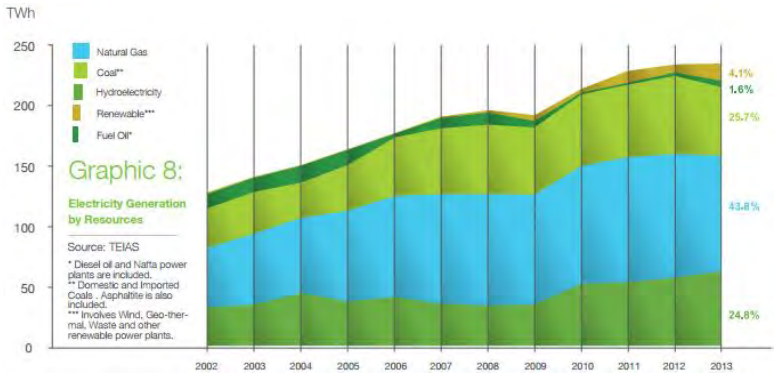

Figure 1.9.1 Energy mix generation in Turkey [16]

The role of the government in formulating and implementing favorable policies for renewable energy development is vital. But the private sector, which has the capacity to mobilize funds, needs to be involved in renewable energy development. The incentives have big importance to accelerate development of renewables in Turkey.

Section 3

1. Wireless charger

Electric signals are the basic concept of the electromagnetic field. These signals are able to carry information and power. The physical principles are based on concepts of near and far fields and radiative propagation.

The near field is referred to as a non-radiative field which acts in close proximity to an antenna more in specific at a distance smaller than one wavelength and fall very fast ($\sim 1/r^3$). The far field is considered to be a radiactive type and it starts propagating form a distance equal two times wavelength up to infinity.

The far field decays slower than the near field ($\sim 1/r$) [17].

So far it has been mentioned what occurs within one wavelength and over two times wavelength. Between these two well defined ranges a combination of near and far field occurs. As it was previously said, those are the basis of telecommunication by mean of electromagnetic waves which are not suitable for power transfer.

In fact, since electromagnetic waves waste the majority of their energy into the free space, they are more suitable for information transmission rather than power transmission.

Wireless power transfer WPT (Wireless electricity) is different from wireless transmission of information. The electromagnetic field allows the energy transfer between two strongly coupled circuits. Actually WPT is based on near field in correlation to the resonant inductive coupling. The coupling through magnetic resonance implies that the two coupled circuits work on their resonant frequency. Two circuits that work in resonance are bonded strongly; whereas the other circuits which could be in proximity, that are not working on the same resonant frequency interact weakly.

Nowadays energy transmission is based on techniques that involve irreplaceable wire. That is what we thought until now. It is true that we cannot replace the wire in all applications but in some daily customs it is possible. What can occur using mechanical contacts is well known. For instance, contacts of removable jacks could ruin themselves, compromising the correct working of the device, producing phenomena such as sparks while unplugging your computer and similar.

Things like the listed ones lead us to research a new method to transmit energy.

In the first place when electrical energy is involved the context has to be safe and this technology, as will be shown, is fully safe.

The main devices that we use are phones, personal computers, tablets and in more recent times, cars. In all these devices a wireless charger can be installed. In this case I will focus on a car charger.

Wireless power transfer (WPT) is a convenient, safe and autonomous mean for plug-in of electrical cars charging . The main advantages of using a WPT are: in first place wire and cables are not required, secondly dirt like dust and grease, weather conditions as snow and rain don't affect the charging process. Moreover WPT doesn't need any device to be handled by users, preventing in that way any possibility of electric shocks.

The inductive power transfer can be considered as more robust than the conductive transmission, since it does not have mechanical parts that need to be connected.

The inductive power transfer uses a magnetic coupling between two coils. The first coil is supplied by a source, typically an inverter operating in high frequency and the second one, the so-called pick-up coil.

The core of WPT are power electronic devices and components which are necessary to convert the power from ac to dc where the last is stored into the batteries.

Firstly, power electronics converters inject harmonics back into the grid. Harmonics have negative effects on the grid since they increase power losses and disturb the normal regime of neighborhood users.

It should be considered that the maximum voltage deviations allowed in Italy are respectively ± 10% Vn for low voltage lines whereas in Europe the deviation is ± 5% Vn and ± 5% Vn for medium voltage lines [18]. Secondly a drawback of power electronics converters is their cost. However, conductive charge system must provide galvanic isolation according to IEC-61851 [19] and this is commonly obtained by using ferrite core high-frequency transformers which also need similar power electronics blocks.

It is useful to recall some basis of induction between coils. Figure 13.1 shows a generic case of coupling between two coils and the theory about this topic will be explained starting from that figure and its equivalent circuit.

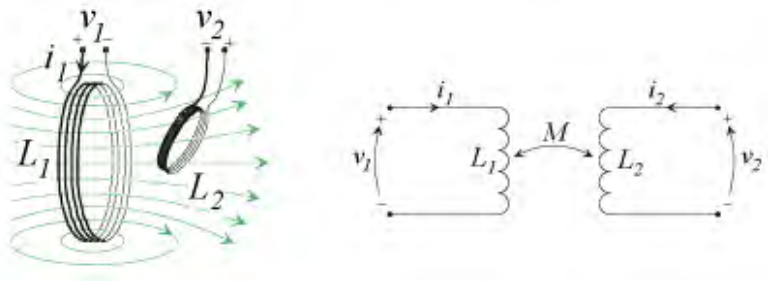

Figure 1.1 Coupling

According to Faraday's Law, a time variable magnetic flux trough a loop-shaped conductor induces an electromotive force emf in the loop.

$$\oint_{E}\overrightarrow{}\overrightarrow{dl}=\frac{d\Phi}{dt} \qquad (13)$$

The time variable field can be generated in several ways. For instance, moving the loop within a non-uniform field or changing the current that generates the field. It is also known that emf is polarised and if the loop-conductor ends are connected together the inducted loop current causes an extra field which stands opposite of the original flux. In other words, this new field tries to stop the original one. This effect goes under the name of Lenz's Law.

One more important law is Biot-Savar's. This law in electromagnetism describes the magnetic field generated by an electric current. Moreover, it describes the relation between magnitude, direction, length, and proximity of the electric current. With this law it is possible to compute the resultant magnetic field B at the position by a steady current I flowing over the path C:

$$B=\frac{\mu_0}{4\pi}\int_C \frac{Idl\times\hat{r}}{|r|^2} \qquad (14)$$

Now, if two coils are in vicinity and in one of them, for instance 1, a time variable current is flowing , that current will produce a magnetic flux coupled with the second coil 2 Φ_B as it is displayed in Figure 13.1. Every time that the current changes into coil 1, efm will change into coil 2 according to Faraday-Lenz's Law. In this conditions a voltage across the terminals of coil 2 occurs.

$$v_2(t) = N_2 \frac{d\Phi_B(t)}{dt} \tag{15}$$

Where n is the number of turns of the coil 2. The Φ_B is linear proportional to the coil current i_1 (see Biot-Savart Low)

$$v_2(t) \propto N_2 \frac{di_1(t)}{dt} \Leftrightarrow v_2(t) = M_{12} \frac{di_1(t)}{dt} \tag{16}$$

The way in which the primary current acts on the coil 2 has been illustrated. Since the secondary current i_2 flows into the coil 2 it will act according to the same laws. Therefore, a voltage across the ends of coil 1 due to the secondary current occurs.

$$v_1(t) = M_{21} \frac{di_2(t)}{dt} \tag{17}$$

It can be shown that M_{12}=$M_{21} = M$. The last parameter is called mutual induction between two coils. If we put M_{12}=$M_{21} = M$ and multiply them per M_{12} and M_{21} , it can be found out that mutual inductance M is proportional to product $N_1 * N_2$, geometry of the coils, their mutual position and surrounding materials that influence the magnetic field distribution. Nearby electric conductors become virtual coil loops in which a certain current is induced. This current is named eddy current and it produces an opposite field with respect to the one they are produced by. If we are considering just one coil or more in general a simple coil, it is possible to define the self inductance as follow:

$$v_1(t) = L_1 \frac{di_1(t)}{dt} \tag{18}$$

where:

$$L1 = \frac{N_1^2 \mu A}{l} \tag{19}$$

The two induction components act simultaneously in a real circuit. Therefore if we consider n number of coils, in each of them we will have the sum of the effects from the current in the coil itself and the currents from the other circuits through mutual inductance.

$$\begin{cases} v_1(t) = L_1 \frac{di_1(t)}{dt} + M \frac{di_2(t)}{dt} \\ v_2(t) = M \frac{di_1(t)}{dt} + L_2 \frac{di_2(t)}{dt} \end{cases} \tag{20}$$

When two coils are considered and one of them is exited by a time varying current a magnetic flux affects the second coil as it is said before. Since the coupling is not perfect and it is always affected by leakage, not all amount of flux go through the second coil. In order to take in account this effect the coupling coefficient k is introduced and it is defined as ratio between mutual inductance an square root of product of two self inductances:

$$k = \frac{M}{\sqrt{L_1 L_2}} \tag{21}$$

1.1. Coupling

In the previous chapters I have described how the system works and in the next one I will apply it to my project.

On the primary side there are: an inverter, the filter box and the coil; whereas on the secondary side there are: the secondary coil, the filter box, the rectifier and the load or storage devices. The most important part in wireless power transmission is constituted by the two interface coils. They, in fact, have a big impact on the efficiency of the circuit. Therefore it is important to choose them according to the appropriate shape and size. The optimum wire for this application is the litz wire as it has a low impedance on high frequency. For a very high frequency, planar and tubular conductors can be considered in order to avoid the skin effect.

The skin effect, which is quantified through skin depth, indicates the distribution of current over the conductor's cross section. Skin depth is defined by the following formula:

$$\delta = \sqrt{\frac{2\rho}{\omega\mu_r\mu_0}} \qquad (22)$$

where, are relative permeability of the conductor, permeability of the free space, resistivity of the material and pulsation respectively.

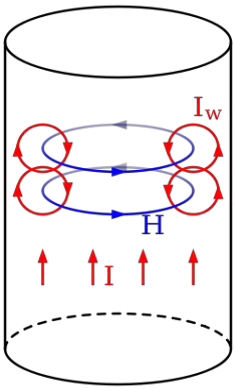

Figure 1.1.1 Skin effect phenomena

In the Figure 1.1.1 above it is shown how the skin effect develops. It is basically due to the eddy current arising from changing H field. In the center of the conductor eddy current has opposite direction with respect to current I flowing into the conductor; whereas near to the surface of the conductor eddy current doesn't work against the current I. Thus the result is that the current density will be greater in proximity of the surface than in the central part of the conductor. When skin effect is present it is necessary to take it in account. One of its effects is that the resistance of the conductor changes.

The effective resistance due to a current confined near the surface of a large conductor thicker than δ, can be solved as if the current flowed uniformly through a layer of thickness δ based on the DC resistivity of that material. A long cylindrical conductor such as a wire, having a diameter D large compared to δ, has a

resistance approximately that of a hollow tube with wall thickness δ carrying direct current. Using a material of resistivity ρ we then find the AC resistance of a wire of length L is:

$$R = \frac{L\rho}{\delta\pi D} \tag{22}$$

Since my project is supposed to work in high frequency it is necessary to find a solution to avoid increases resistance due to skin effect. Litz wire can contribute to reduce skin effect. It consists of many thin wire strands, individually insulated and twisted together, following one of several carefully prescribed patterns, often involving several levels of elementary thin wire. As previously introduced, power is transmitted to the load via magnetic coupling between two coils. The efficiency of systems is defined as ratio between the output and input quantities. In the specific case these quantities are power delivered to the load and power given in input of the system. All devices between input and output are affected by losses. Therefore well designed devices are necessary.

In order to find the coupling coefficient firstly it is necessary to calculate the mutual inductance between two coils and the self inductance of the coils. Mutual inductance is calculated by Neumann's equation which is expand below.

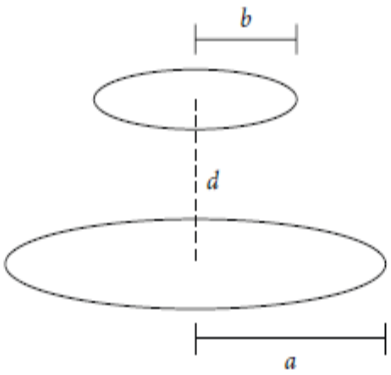

Figure 1.1.2 Generic coil coupling

$$M = \frac{\mu}{4\pi}\iint \frac{\cos(\varepsilon)}{r} ds ds' \tag{24}$$

Where ds and ds' are the section where the integral is calculated whereas r is the distance between these two section.

$$r = \sqrt{a^2 + b^2 + c^2 - 2a\cos(\phi - \phi')} \tag{25}$$

$$\varepsilon = \phi - \phi' \quad ds = ad\phi \quad ds' = bd\phi' \tag{26}$$

If we substitute (25), (26) formulas in (24):

$$M = \frac{\mu}{4\pi}\iint_0^{2\pi} \frac{ab\cos(\phi - \phi')}{a^2 + b^2 + c^2 - 2a\cos(\phi - \phi')}\, d\phi d\phi' \tag{27}$$

The last formula can be rewritten using elliptic integrals of first and second order in order to be implemented in MATLAB.

$$M(m) = \frac{2\mu\sqrt{ab}}{m}\left[\left(1 - \frac{m^2}{2}\right)K(m) - E(m)\right] \tag{28}$$

K(m) and E(m) are elliptic integrals of first and second kind which are available as tools in MATLAB. The parameter m, which is variable in the last equation, is a geometrical description of the coils and distance between them.

$$m = \sqrt{\frac{4ab}{(a+b)^2+d^2}} \tag{28}$$

As long as its value remains ranged between 0 and 1.

From these formulas it is possible to obtain the power transferred to the load in air core system:

$$P = \frac{\omega k^2 \mu A}{l}(N_1 I_1)^2 \tag{30}$$

Those formulas describe in a theoretical way the behavior of the circuit. However the most important part of a project is its realization. In some cases measured results diverge significantly from theoretical prediction. Therefore it is necessary to describe well all the parameters of the circuit.

2. The project of the charger

My project started with the idea of making a wireless charger and a model based on the transformer concept. The charger is supposed to charge the battery of an electrical car without any contact. Air gap across which it is necessary to transfer the power was set to be 5 cm. The first coils of the model have a diameter of 10 cm and several number of turns ware tested.

Figure 2.1Sample of the coil used

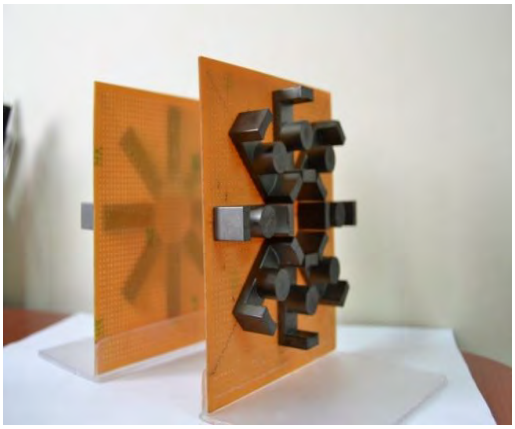

Figure 2.2 Support for the coils with ferromagnetic material

In the Figures 2.1 and 2.2 above it is shown the first coil used for the charger. The wire that is used for the coils is copper wire with a nominal diameter of 0,5 mm. The choice of using this wire was made because on the frequency of 25kHz it causes no problem with skin effect. For this project are used also 8 ferrite element per side in order to concentrate the magnetic flux. Since the ferrite elements doesn't close well magnetic loop lines I noticed that those elements doesn't contribute for a better coupling and has not been used for further experiments.

In the first test a half-bridge inverter was used. The number of turns of the coils was 40 and 20 for primary and secondary coil respectively. During this test it was noticed that the system's signals produced noise. To avoid this problem the circuit was provided by the low pass filter which also contribute for a better energy transmission.

Since the operating frequency is high and noise content is also high, the capacitance across the output drains a relatively high current and heats up itself.

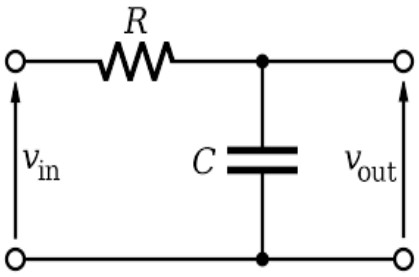

Figure 2.3 Low pass filter scheme

In the second model that was realized, two concentric coils per each, primary and secondary side were adopted. This topology of the circuit was aimed at improving the coupling between primary and secondary side. Moreover, mutual inductance M rose with two concentric coils but the coefficient k was still low because L of the coils, which is on denominator in the formula of k.

The next step was to design a full bridge inverter. For this circuitI used four IRF540N which are MOSFET. The most important part of this circuit is driving the circuit; mine is realized using two IR2106. As it will be shown in Figure 12.1 this full bridge circuit gives a good quasi square signal.

Our load is an incandescent lamp which works in DC current. Before the lamp a rectifying circuit is needed. As rectifying circuit a Graetz bridge is used.

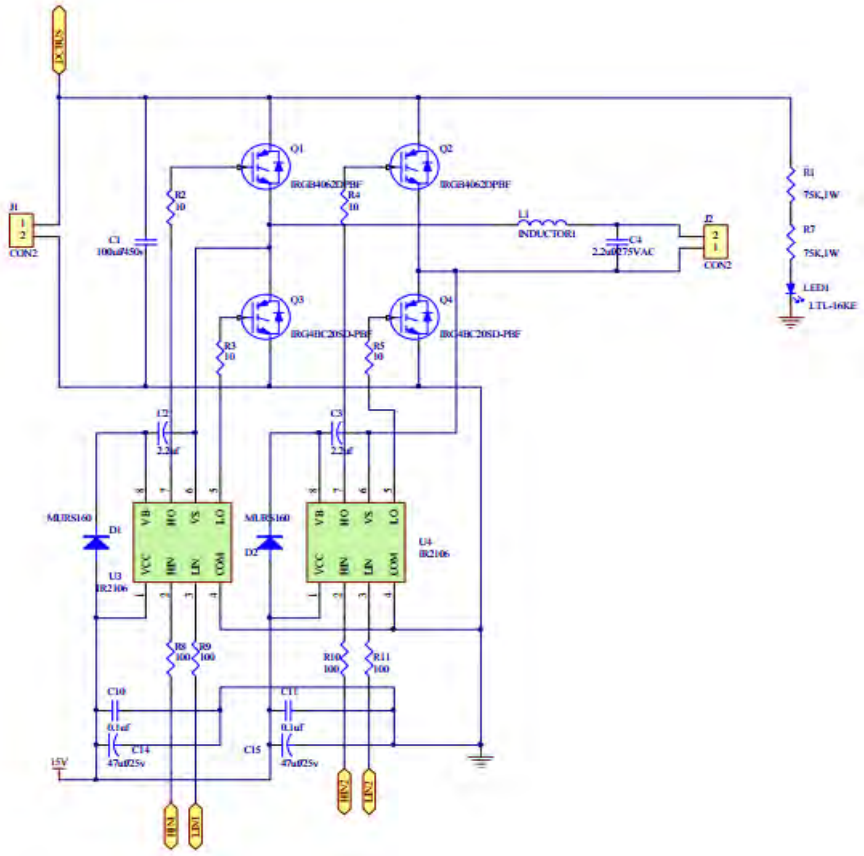

Figure 2.4 IR2106 full bridge

3. Results

Using a full bridge inverter with MOSFETS which are driven by IR2106 and PWM modulation waveforms of the Figure 3.1 are obtained.

All the waveforms are displayed together in Figure 3.1 for an easier valuation. The letters on the left side indicate the zero point and those one the right one indicate the time evolution of the signal.

Waveform A shows PWM signal which limited and oscillates between 0 and 5 Volts. PWM is generated by a signal generator.

B indicates the voltage across the primary coil. As it is possible to see in the figure this signal has 20 Vp. It was noticed that without the ferrite components the voltage on the secondary coil doesn't change but the current rises on equal load. Wave C indicates the voltage of the secondary coil. This wave lag with respect to the primary coil voltage. It is also noted that the delay depends slightly on the air gap. In fact, with an air gap of 3 cm wave C is shifted on the right of 5us. Finally, wave D indicates the rectified voltage. It is possible to see a small amount of ripple.

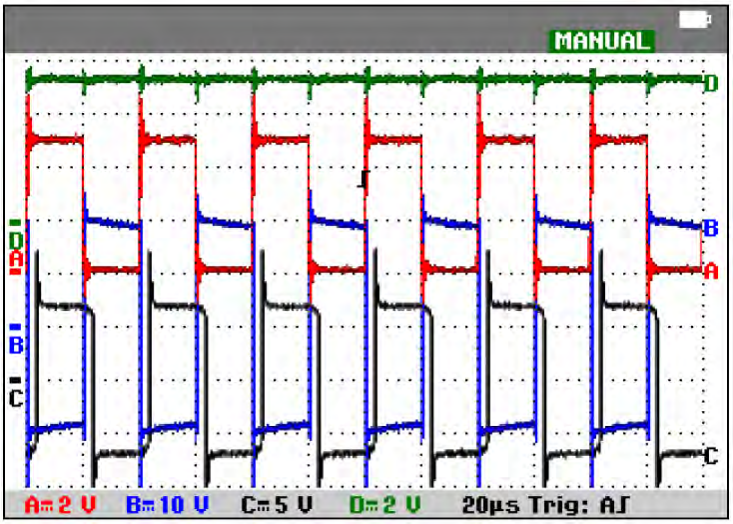

Figure 3.1 Wave shapes

3.1. Inverter

The inverter was reviewed one more time in terms of power with respect to the previous. This inverter is a prototype designed to supply a power of about 100 W. In first place the same scheme of the precedent inverted has been made on PCB Figure 3.1.2 In Figure 3.1.1 it is possible to see block scheme of the system which has been developer partially.With Proteus software the PCB was designed and den developed. In order to make this inverter independent a PIC controller has been involved in the circuit. With this PIC controller it is also possible to change in every moment the working conditions of inverter in terms of frequency. Moreover PIC is able to collect data of current and voltage and show it on display. Furthermore in future it will be possible to download data in a computer form micro controller.

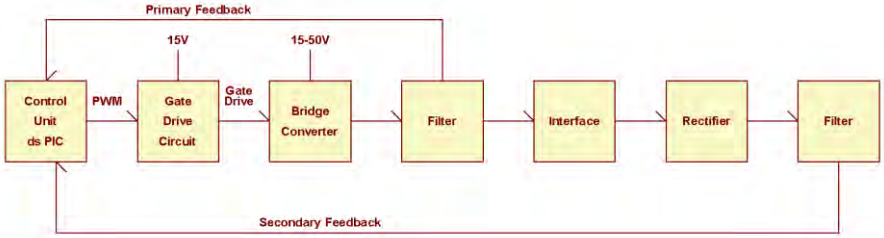

Figure 3.1.1 Block scheme of the system

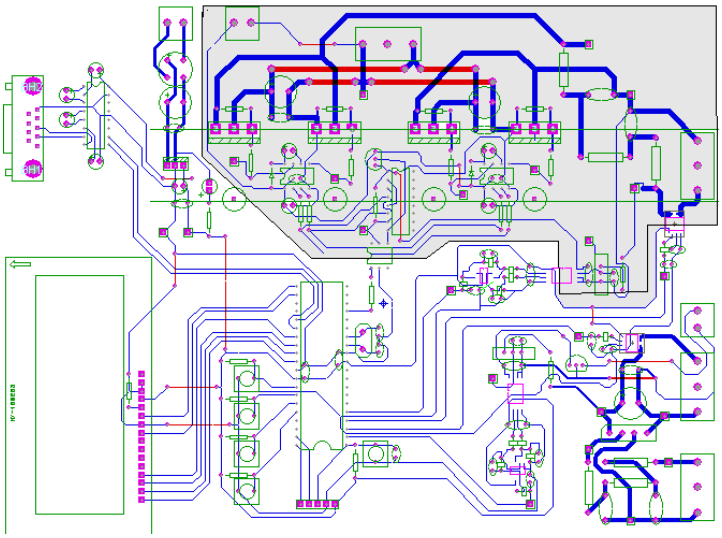

Figure 3.1.2 PCB layout

It can be noticed a highlighted grey area which delimit power part of the circuit with its control. Power part of the circuit is electrically isolated to prevent voltage impulses issues in driving circuit. Command impulses coming from PIC are transmitted through a couple of photo-diode and photo-transistor to the integrate circuit which spread the signals to H-bridge. Composed circuit is the one of the Figure 3.1.3 . The PCB board was designed using Proteus software. For esthetic and practical reasons it has been chosen to install Mosfets under the board with a big single radiator.

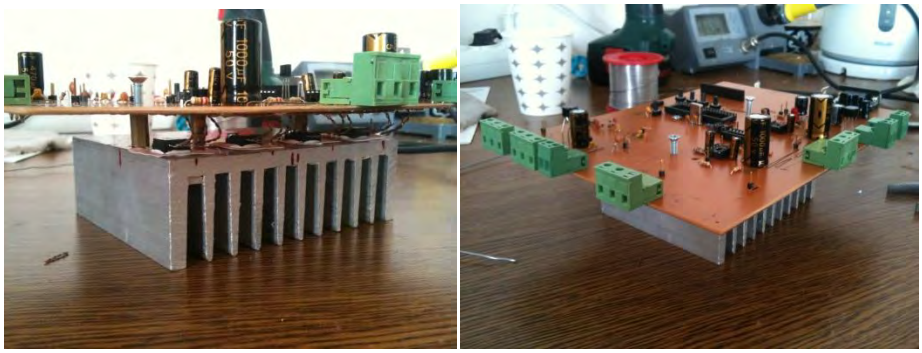

Figure 3.1.3 Inverter circuit

3.2.Rectangular coil

In order to move toward the final aim of the project a wider rectangular coils has been designed. Area of the coil has been enlarged to reduce misalignment problem and also to increase transmittable power.
Both primary and secondary coils are make with the same 0,5 mm copper wire and dimensions of about 0.25x0.15 m Figure 3.2.1. Following wave-forms are for the coils which have 30 and 10 turns for primary and secondary side respectively.

Figure 3.2.1 Rectangular coil

First test

In the first test primary coil supplies secondary across an air gap of 20 mm. The load in all experiments is a bulb with resistance of 8 Ω. Data and wave forms of primary and secondary voltage follow. It is important to notice that especially primary compensation capacitor mast have a high isolation voltage with respect to the voltage of the circuit.

	Primary	Secondary
N	30	10
L [uH]	420	27
R [Ω]	2,5	1
f [kHz]	24	24
C comp [nF]	100	1000
D [mm]	0,5	0,5
d [mm]	20	
misalg. [%]	0	
I [A]	3	2,8
V [V]	33,4	20
VC1 [V]	205	
P [W]	100,2	56
Eff [%]	0,56	
NB: Capacitors are isolated for 1600V DC		

Table 3.2.2 General data and first test results

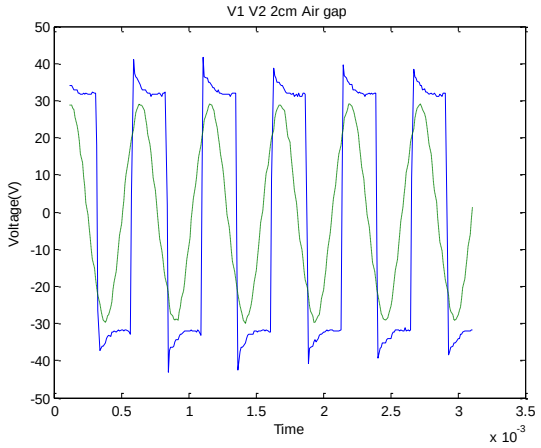

Figure 3.2.3 V1 and V2 waveforms 20 mm air gap

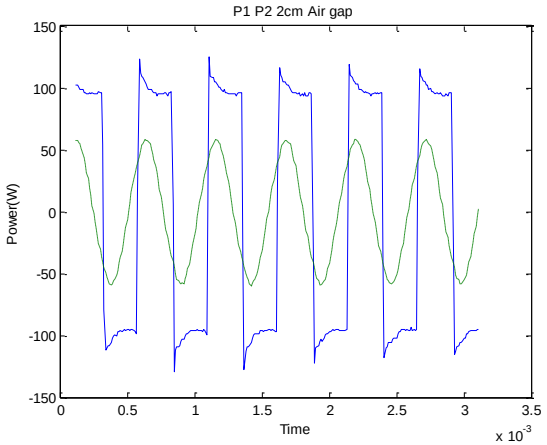

Figure 3.1.2 P1 and P2 waveforms 20 mm air gap

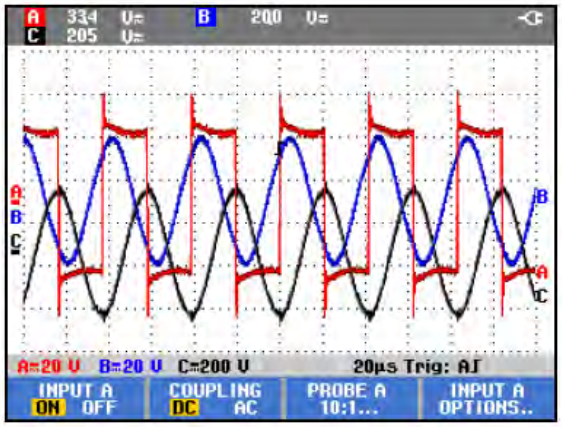

Figure 3.1.3 Scope screen shot 20 mm air gap

It is possible to notice that the secondary voltage wave has a small delay because of the transmission of the power between coils.

Second test

In the first test primary coil supplies secondary across an air gap of 40 mm. Data and wave forms of secondary and primary voltage follow

misalg. [%]	0,00	
I [A]	3,00	2,60
V [V]	26,60	15,40
VC1 [V]	213,00	
P [W]	79,80	40,04
Eff [%]	0,50	

Table 3.1.2 Second test data

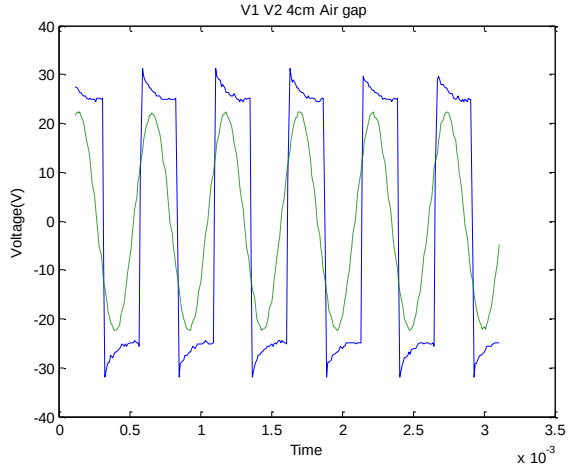

Figure 3.1.4 V1, V2 for 40 mm air gap

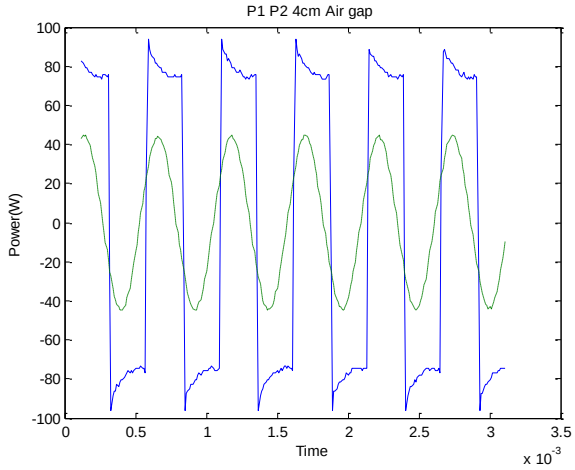

Figure 3.1.5 P1, P2 for 40 mm air gap

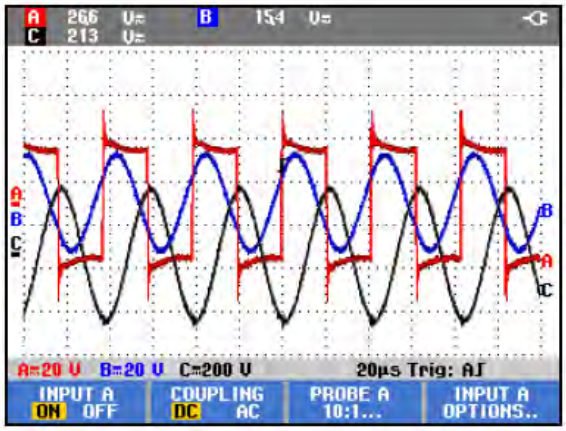

Figure 3.1.6 Scope screen shot 40 mm

Third test

In the first test primary coil supplies secondary across an air gap of 70 mm. Data and wave forms of secondary and primary voltage follow. If we take a closer look on the waveforms it is possible to see that the delay between primary and secondary voltage decrease when the distance increase. In particular for the distance of 70 mm between coils waveforms are in phase.

misalg. [%]	0,00	
I [A]	3,00	2,40
V [V]	27,50	11,30
VC1 [V]	262,00	
P [W]	82,50	27,12
Eff [%]	0,33	

Table 3.1.3 70 mm air gap experiment data

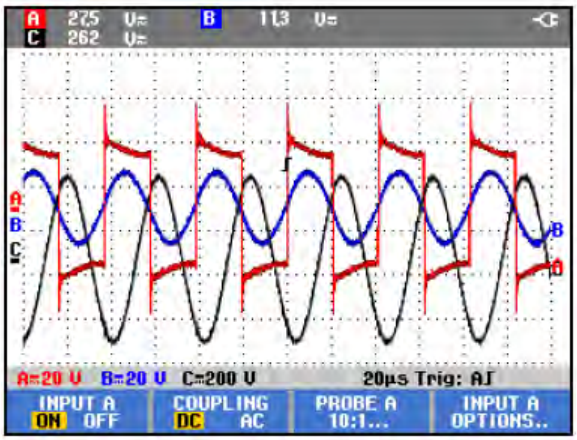

Figure3.1.7 Scope screen shot 70 mm air gap

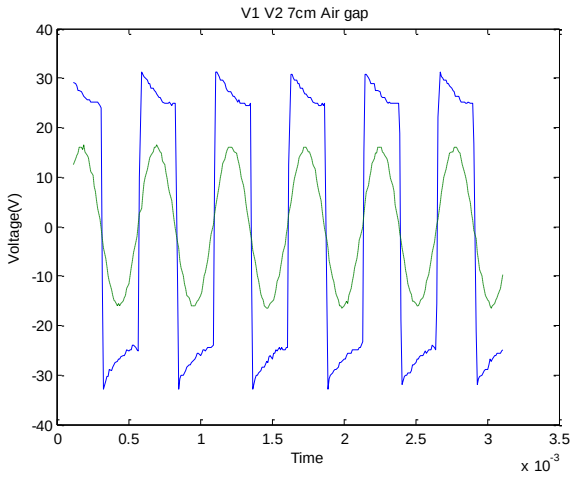

Figure 3.1.8 V1, V2 for 70 mm air gap

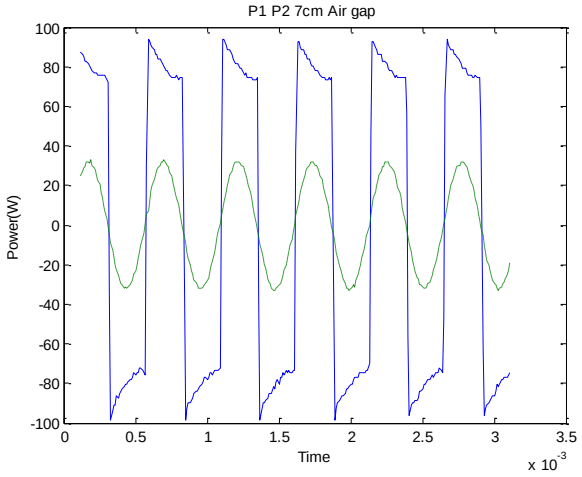

Figure 3.1.9 P1, P2 for 70 mm air gap

Fourth and fifth test

In following two tests we simulate misalignment between coils of 30% and 50%. Also in this case it is possible to see that phase between voltage waves changes and in 50 % misalignment two waves are in phase. Air gap for these experiments was set on 20 mm.

misalg. [%]	30,00	
I [A]	3,00	2,40
V [V]	26,50	15,30
VC1 [V]	213,00	
P [W]	79,50	36,72
Eff [%]	0,46	

Table 3.1.4 20 mm, 30% misalignment experiment data

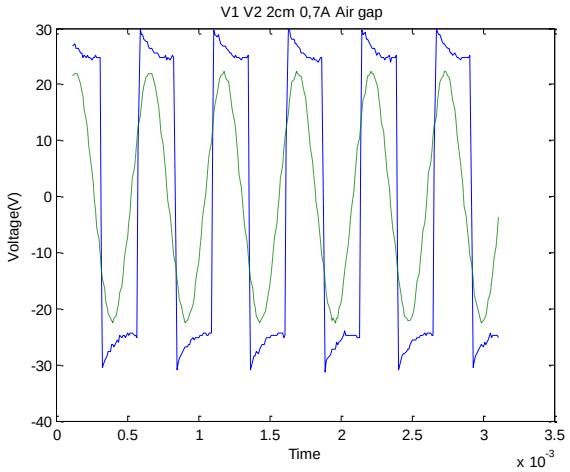

Figure 3.1.10 V1, V2 for 20 mm air gap and 30% misalignment

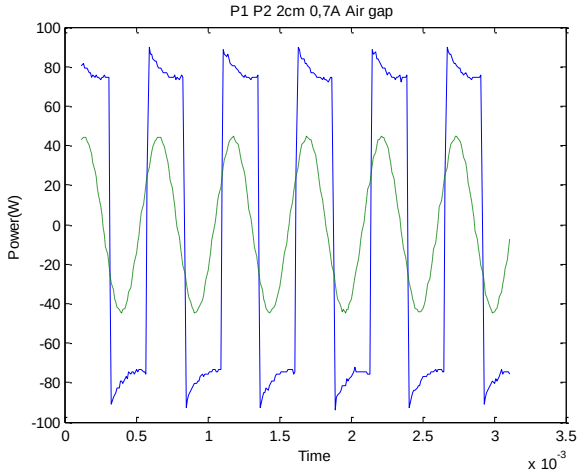

Figure 3.1.11 P1, P2 for 20 mm air gap and 30% misalignment

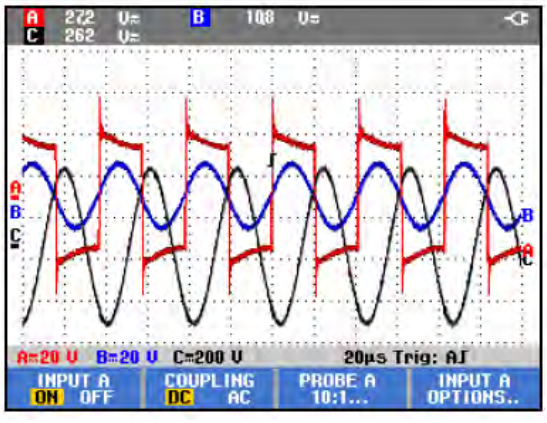

Figure 3.1.12 Scope screen shot 20 mm, 50% misalignment

misalg. [%]	50,00	
I [A]	3,00	2,20
V [V]	22,20	10,80
VC1 [V]	262,00	
P [W]	66,60	23,76
Eff [%]	0,36	

Table 3.1.5 20 mm, 50% misalignment experiment data

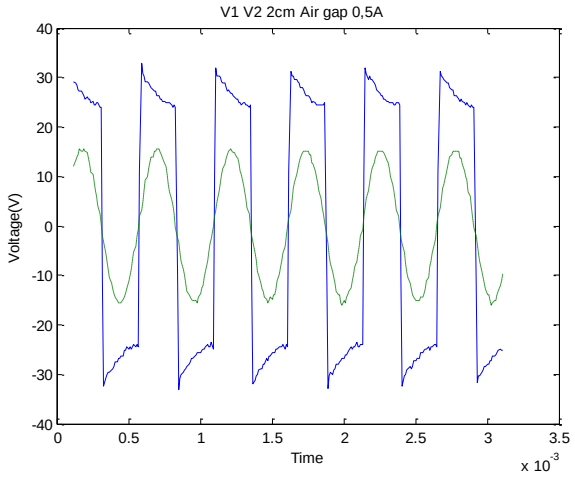

Figure 3.1.13 V1, V2 for 20 mm air gap and 50% misalignment

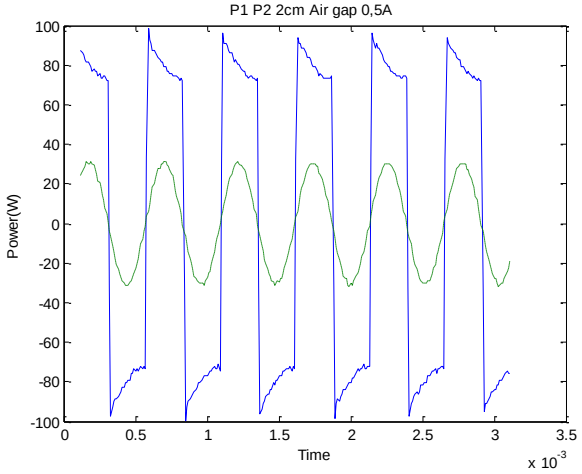

Figure 3.1.13 P1, P2 for 20 mm air gap and 50% misalignment

4. Compensation

For a better transmission of the power between the two parts of the system it is important to implement a compensation block on both sides of the circuit. These compensator, which are mainly capacitance, are supposed to work in resonance with the inductance of the coil. In this theoretically way the added capacitance will erase the inductance of the circuit and the remaining impedance will be a pure resistance. In other words phase shift of the current with respect to the voltage will be zero. There are four main compensation circuits which are shown in Figure 13.1 .

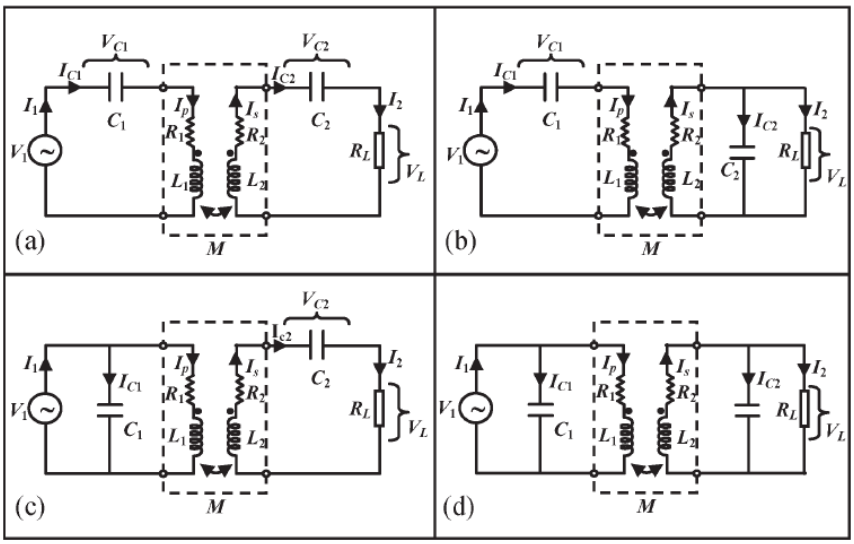

Figure 13.1 Compensation schemes

For the project it was used a compensation scheme with capacitor in series with the coils on both, primary and secondary part.

As you can see the concept of this techniques is similar to a trafo. Suitable for short distance and capability of hundreds kW. But the problem is frequency. In other words high frequency is necessary because the active power is proportional to the frequency. With high frequency also impedence of the circuit rise. In order to transmit energy between coils it is necessary a compensation filter. Indeed in my project it was necessary to implement the filter since the power I could transmit was little without the filter. Moreover the coils with the filter doesn't heat up even with 3 Amperes circulating in the primary coil. One of the biggest problems was the isolation voltage of the filter capacitor. In particular on the primary side I had to use a capacitor isolated 1600 V.

Entire charger scheme is shown if Figure 13.2.

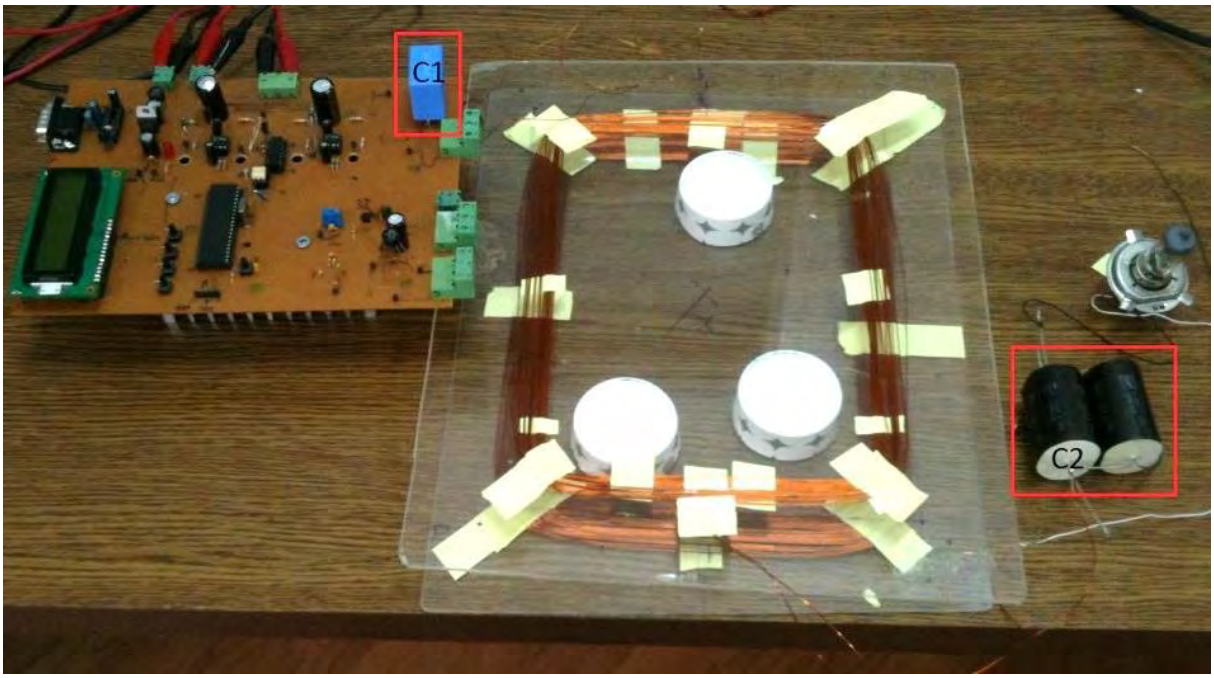

Figure 13.2 Inverter, coils and compensation capacitors

Conclusions

In this study it is shown what the photovoltaic effect is and how we can exploit it.

In first place I drawn the picture of how the conversion occurs from an ideal point of view. In the past sections all imperfections and losses of the material were neglected in order to conduct the study. Some of the materials were deeply investigated with the aim to show what are the conditions to satisfy to obtain desired effect. Correct design, carefully fabrication and post fabrication processes such as texturing and low reflective materials deposition are fundamental for a efficient device.

Materials widely known as Silicon and was taken as specimen. Then, in order to obtain a more real object of study all the imperfection and different characteristics of materials that negatively contribute to the efficiency were introduced one by one. For a further improvement and to involve also the recent progresses of technology I have analyzed materials that use Perovskite concept. Such materials experienced an extremely fast development and they constitute a new promising field for research.

Since the PV technology is spreading all around the world I thought that it could be useful to find the perfect subsiding system taking advantage of the experience of developed countries. In order to develop this standardization idea I conducted a comparative study between Turkey and Italy. Referring to Italy as the developed country, at first the Italian case was illustrated and then the Turkish one. At the end of the illustration of the different subsiding systems, their results were also discussed. Fınally, what emerged from my comparison is that Turkey has recently started introducing renewable energy in its market and renewable resources are in great amount.

After conducting the comparative study I introduced the project of a wireless power transmission. I was motivated by the challenging topic and by the idea of experiencing some practical work after many theoretical analysis .

Indeed, this prototype of wireless charger allowed to me to face the meaning of designing a circuit and side systems that permit a correct operation of the project. A high frequency inverter was designed in order to supply the coils through which the power (will) flows. Different shapes and sizes were tested and all of them were tested in laboratory.

Several inconvenients were faced during the development of the project which were systematically solved. Further improvements for this application should be made, especially on the inverter in order to obtain a good waveform from the it and on the primary and the secondary filter . Aiding a shield of soft magnetic material could contributed to improve the low efficiency of this first study. Further research on the topic could improve the results and efficiency of the project.

Riassunto

Il presente lavoro ingloba uno studio su diverse tematiche e si sviluppa come segue: la prima sezione si concentra sulla storia e lo sviluppo delle tecnologie fotovoltaiche, la secondo sezione illustra lo studio comparativo tra l'Italia e la Turchia in materia di sviluppo delle tecnologie fotovoltaiche e la terza e ultima sezione descrive il progetto e la realizzazione del modello di carica batterie senza fili.

Per più di due decenni il fotovoltaico è stato il campo di maggior ricerca nell'ambito del rinnovabile. Nella parte iniziale della prima sezione ho introdotto la più usata e studiata innovazione nel fotovoltaico. Nel primo capitolo ho esaminato l'effetto fotovoltaico nei suoi punti cruciali. Successivamente ho introdotto le principali problematiche della tecnologia fotovoltaica introducendo anche le possibili soluzioni a questi difetti. La luce, il suo intrappolamento e le perdite ottiche sono descritte e spiegate nel secondo paragrafo della Sezione I. In questo paragrafo sarà possibile comprendere che cos'è la luce e come si propaga nello spazio e nei diversi corpi. Ciò è necessario per capire successivamente quale parte dello spettro produce effettivamente l'effetto fotovoltaico e quale parte di tale spettro può essere utilizzata efficientemente. Inoltre nella Sezione I seguirà il quarto paragrafo nel quale sono analizzati emettitori di elettroni come il silicio; questo paragrafo affronterà le questioni riguardanti la struttura, le proprietà e le regole per una corretta progettazione della cella fotovoltaica. Oltre ad un'attenta descrizione delle regole, saranno menzionate anche le tecniche per il miglioramento delle prestazioni della cella. I paragrafi successivi (dal 5 al 7 della Sezione I) sono dedicati ad illustrare le tecnologie più recenti come le celle a giunzione multipla e le celle basate sul materiale Pervoskite. Quest'ultimo è illustrato nel dettaglio evidenziando il suo sviluppo molto rapido. Paragrafo 8 è l'ultimo paragrafo di questa Sezione illustra la prospettiva dell'energia proveniente da fonti basate sul solare confrontando l'andamento con diversi Paesi.

La Sezione II è strettamente legata al contesto in cui ho condotto la mia ricerca. Questa sezione evidenzierà il confronto tra il sistema di incentivazione italiano e quello turco al fine di contribuire alla realizzazione di un sistema adeguato di incentivazione per una diffusione su larga scala.

Infine, la Sezione III riguarda la mia progettazione di un carica batterie senza fili. In questa sezione ho illustrato la progettazione di un prototipo di carica batterie per veicoli elettrici cercando di ottimizzare la dimensione e la forma delle bobine primaria e secondaria per massimizzare la potenza trasmissibile. Successivamente ho riportato i risultati sperimentali svolti in laboratorio.

Bibliography

1] “Solar Energy,” 2014.

[2] P. H. A. N. D. B. O. O. K. Of, “Phot Handbook of Photovoltaics : Section Finder.”

[3] A. Luque and S. Hegedus, *Handbook of Photovoltaic Science*. .

[4] N.-G. Park, “Perovskite solar cells: an emerging photovoltaic technology,” *Mater. Today*, vol. 00, no. 00, pp. 1–8, Aug. 2014.

[5] T. Qi, I. Grinberg, J. W. Bennett, Y.-H. Shin, A. M. Rappe, K.-L. Yeh, and K. a. Nelson, “Studies of Perovskite Materials for High-Performance Storage Media, Piezoelectric, and Solar Energy Conversion Devices,” *2010 DoD High Perform. Comput. Mod. Progr. Users Gr. Conf.*, pp. 249–258, Jun. 2010.

[6] Z. Yang and W.-H. Zhang, “Organolead halide perovskite: A rising player in high-efficiency solar cells,” *Chinese J. Catal.*, vol. 35, no. 7, pp. 983–988, Jul. 2014.

[7] P. Tre and C. Energia, “Il Primo Conto energia (D.M. 28 luglio 2005, modificato dal D.M. 6 febbraio 2006),” 2013.

[8] “Gestore Servizi Energetici (GSE).” .

[9] D. I. C. Con, “IL MINISTRO DELL ’ AMBIENTE E DELLA TUTELA modificazioni , gli interventi che prevedono l ’ installazione di impianti solari fotovoltaici aderenti o integrati nei tetti degli edifici con la stessa inclinazione e lo stesso orientamento della falda e i cui ,” pp. 29–50, 2010.

[10] C. Area, “Fifth feed-in scheme,” 2012.

[11] V. D. Aosta, “Totale dei risultati del conto energia,” 2013.

[12] P. C. Energia and S. C. Energia, “Numerosità Potenza Cumulata (kW) Grafici della numerosità e della potenza totale degli impianti mensilmente entrati in esercizio con il Conto Energia . Potenza Mensile (kW).”

[13] D. Kaya and F. Çanka Kılıç, “Renewable Energies and Their Subsidies in Turkey and some EU countries- Germany as a Special Example,” *Int. Environ. Appl. Sci.*, vol. 7, no. 1, pp. 114–127, 2012.

[14] S. G. Gok and R. Kavasoglu, “The renewable energy policy of Turkey,” *4th Int. Conf. Power Eng. Energy Electr. Drives*, no. May, pp. 1334–1339, 2013.

[15] F. C. Kilic, “Recent renewable energy developments, studies, incentives in Turkey,” *Energy Educ. Sci. Technol. Part A Energy Sci. Res.*, vol. 28, no. 1, pp. 37–54, 2011.

[16] S. Allen, G. Perez-cruz, P. R. Vail, J. B. Anderson, and M. a Thomas, “Table of Contents Table of Contents,” 1892.

[17] Johnson I. Agbinya, “Wireless Power Transfer,” 2012.

[18] F. D. I. Ingegneria, “Power quality.”

[19] J. L. Villa, J. Sallán, J. Francisco, S. Osorio, and A. Llombart, “High-Misalignment Tolerant Compensation Topology For ICPT Systems,” vol. 59, no. 2, pp. 945–951, 2012.